Scanning Microscopy

Volume 9 | Number 3 Article 1

9-14-1995

Interactions of Low-Energy Electrons with Atomic and Molecular Solids

Leon Sanche
Universite de Sherbrooke, lsanche@courrier.usherb.ca

Scanning Microscopy, Vol. 9, No. 3, 1995 (Pages 619-656) 0891-7035/95$5.00+.25
Scanning Microscopy International, Chicago (AMF O'Hare), IL 60666 USA

INTERACTIONS OF LOW-ENERGY ELECTRONS WITH ATOMIC AND MOLECULAR SOLIDS

Léon Sanche*

MRC Group in the Radiation Sciences, Faculty of Medicine,
Université de Sherbrooke, Sherbrooke, Québec, Canada J1H 5N4

(Received for publication April 27, 1995 and in revised form September 14, 1995)

Abstract

Low energy electrons are involved in a large number of analytical techniques for material analysis either as secondary particles or as the primary excitation source. The interaction of these electrons near the surface of solids can be investigated with high-resolution low-energy electron-beam techniques. The results of experiments performed on atomic and molecular solids in the range 0-30 eV with such techniques are reviewed in the present article. The major types of experiments are briefly described and examples of the results obtained from them are given to illustrate the basic mechanisms which control the electron-solid interactions and to provide a description of the basic degradation processes involved during sample irradiation. It is shown that elastic and quasi-elastic scattering of slow electrons can be described in terms of band structure parameters whereas inelastic scattering is usually governed by the formation of transient anions. These anions can decay by stabilization, by producing vibrationally and electronically excited molecules, or by dissociating into a stable anion and a neutral radical. These latter species usually initiate other reactions with nearby molecules causing further chemical damage. It is shown that the damage caused by transient anions can be controlled by modifying its molecular environment.

Key Words: Low energy electrons, secondary electrons, rare gas solids, molecular solids, transient anions, beam damage, organic solids, dissociative attachment, vibrational excitation, excitons.

*Contact for Correspondence:
Léon Sanche, address as above.
Telephone number: (819) 563-5555, Ext. 4678
FAX number: (819) 564-5442
E-Mail: lsanche@courrier.usherb.ca

I. Introduction

When a charged particle enters a solid with high velocity, it ionizes the medium, producing a distribution of excited atoms and molecules, ions and secondary electrons. These latter are created in large quantities ($\sim$4/100 eV) and carry most of the energy of the fast primaries. Secondary electrons have low energies with a distribution lying essentially below 70 eV and a most probable energy around 10 eV [128]. At those energies, electrons have their highest cross-section for scattering by atoms and molecules [114]. Hence, they interact rapidly and within a very short range ($\sim$5-100 Å) in the irradiated medium, where they generate highly reactive species which initiate chemical reactions. Secondary electrons are involved in electron microscopy [38] as well as in many techniques of microanalysis which utilize fast charged particles as the primary excitation source. Therefore, the description of the processes involved in these techniques cannot be complete without a description of the action of secondary electrons within solids and at their surfaces. Such a description is particularly important for techniques in which the probe particles are secondary electrons [203] or products formed by them.

As shown in this article, information on the behavior of secondary electrons can be obtained from experiments which directly probe the interaction of low-energy electrons with condensed matter. The results of such experiments are directly related to high resolution electron energy loss (HREEL) spectroscopy, scanning tunneling microscopy (STM), low energy electron diffraction (LEED), electron stimulated desorption (ESD) and Low energy electron microscopy (LEEM; for a bibliography on LEEM and related techniques, see Griffith *et al.* [46]), since in these techniques the primary particle is a low-energy electron. These and other acronyms are defined in Tables 1 and 2. Table 1 lists different methods of analysis arranged according to the role of low energy electrons in the detection process (for a short description of most of these methods see Garten and Werner [37]). Within group A (Table 1), secondary

Table 1. Methods of analysis.

A. Methods in which low energy electrons are produced as secondary particles	
CPAA	Charged particle activation analysis
EELS	Electron energy-loss spectroscopy
EPXMA	Electron probe x-ray microanalysis
EXAFS	Extended x-ray absorption fine structure
ISS	Ion scattering spectrometry
MEED	Medium energy electron diffraction
PIXE	Proton-induced x-ray emission
RHEED	Reflected high energy electron diffraction
SEM	Scanning electron microscopy
STEM	Scanning transmission electron microscopy
TEELS	Transmission electron energy-loss spectroscopy
TEM	Transmission electron microscopy
B. Methods in which all or some of the detected particles are low-energy electrons	
AES	Auger electron spectrometry
PEEM	Photoelectron emission microscopy
SAM	Scanning Auger microprobe
SES	Secondary electron spectroscopy
UPS	Ultraviolet photoelectron spectroscopy
XPS	X-ray photoelectron spectroscopy
C. Methods using low-energy electrons as the primary source	
ESD	Electron stimulated desorption
HREELS	High resolution electron energy loss spectroscopy
LEED	Low energy electron diffraction
LEEM	Low energy electron microscopy
LEET	Low energy electron transmission spectroscopy
STM	Scanning tunneling microscopy

electrons are not directly analysed and information on their action is mostly needed to understand the details of sample damage. Nevertheless, this is an important issue as several types of damage have been observed in electron microscopy (dissociation, desorption, reduction, polymerization, oxidation, carburization, etc.) [136]. The details of the damage mechanisms are still poorly understood and not sufficiently documented to predict damage rates in a variety of materials [136]. The methods listed in group B (Table 1) examine surfaces by exciting the target with a flux of particles and analyzing the energy distribution of the emitted electrons. In the methods listed in the last group (C, Table 1) the primary particles are low-energy electrons; in this case, the transmitted or emitted electrons or the emitted neutrals or ions are analysed.

TABLE 2. List of acronyms used in the text.

a-STE	Atomic self trapped exciton
CDOS	Conduction band density of states
DD	Dipolar dissociation
DEA	Dissociative electron attachment
ESD	Electron stimulated desorption
FE	Free exciton
FWHM	Full width at half maximum
IC	Injection curve
KE	kinetic energy
ML	Monolayer
MP	Metastable particle
m-STE	Molecular self-trapped exciton
PDI	Post-dissociation interaction
RG	Rare gas
TOF	Time of flight
UV	Ultraviolet

The aim of this article is to explain the main aspects of the interaction of secondary (i.e., low-energy) electrons with atomic and molecular solids and provide pertinent examples from experimental results which involve the direct interaction of a low-energy electron beam with such solids or with specific molecules condensed on their surfaces. The review of the literature is limited to experimental data obtained by the impact of low energy (0-30 eV) electron beams with thin films of atomic, molecular and organic solids.

Relevant concepts to describe the behavior of low energy electrons within molecular solids are given in section **II**. In section **III**, the type of experiments which generated the reviewed experimental information are briefly described. In the subsequent sections (**IV to VI**), the results of experiments on energy transfer by electron impact are reviewed. These include phonon creation and vibrational and electronic excitations. Specific examples are provided to illustrate the most important interactions. Molecular dissociation caused by electron excitation and attachment is described and reviewed with pertinent experimental results in section **VII**. The mechanisms involved in electron trapping are described in section **VIII**. Examples of the products formed as the result of reactions of the dissociation fragments produced by low-energy electrons are provided in section **IX**. All results are explained with emphasis on the fundamental mechanisms which govern energy losses and molecular dissociation.

II. Interaction of Low-Energy Electrons with Matter

When an electron scatters or reacts at the surface or within a solid, a description of the phenomenon is highly dependent on its wavelength. If the electron wavelength is short in comparison with the "diameter" or separation

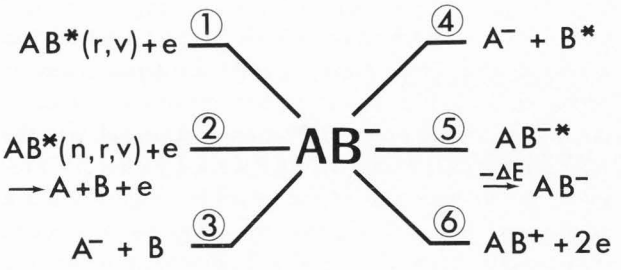

Figure 1. Decay channels of a temporary anion AB^-.

---

of the elementary constituents of condensed matter, the electron can be considered to interact approximately independently with each atom or molecule. Thus, the scattered amplitude within or outside a solid or a liquid is considered as the sum of the individually scattered waves. This concept is no longer valid at low energies, where the electron wavelength is of the order of the interatomic or intermolecular distances. In this case, the electron interacts "collectively" with many targets and the scattered intensity must be derived from the sum of the interactions between the electron and each of the elementary constituents of condensed matter. Solving the Schrödinger equation with such a potential is a much more tedious task than for the case of the single-electron-target system. Therefore, it is more desirable to describe electron scattering in condensed phases with models of the most prominent interaction. Recent papers by Fano [32], Fano and Stephens [33], and Mills [112] outline the relevant concepts and theoretical procedures required to describe the action of slow electrons in condensed media. Earlier attempts are to be found in the theoretical work of Fröhlich [34], Fröhlich and Platzman [35], and Magee and Helman [83].

Description of the scattering process in terms of intramolecular resonant and direct mechanisms is an approach which has proven successful in describing the interaction of low energy electrons with **molecular solids.** With this approach, it has often been possible to explain structures in the energy dependence of an inelastic cross-section (or a signal proportional to that cross-section) by invoking the formation, at specific energies, of transient anions within the solid or near its surface. Comparison with gas-phase data is most useful in identifying the resonant state and in investigating the modifications to the characteristics of the isolated transient anion induced by the presence of neighboring targets. Other non-resonant features in the energy dependence of the cross-sections can usually be explained by specifying which part of the interaction potential is dominant. Resonances occur when the scattered electron resides for a much longer time than the usual scattering time in the neighborhood of a target atom or molecule. From an atomic or molecular orbital perspective, a resonant state may be considered as a negative ion formed by an electron which temporarily occupies an orbital of the target. This concept leads to the definition of two major types or categories of resonances or transient anions [1, 183, 184]. If the additional electron occupies a previously unfilled orbital of the target in its ground state, the transitory state is referred to as a single particle resonance. The term "shape" resonance applies more specifically when temporary trapping of the electron is due to the shape of the electron-molecule potential. When the transitory anion is formed by two electrons occupying previously unfilled orbitals, the resonance is called "core-excited" or may be referred to as a two-particle, one-hole state.

When the projectile electron is temporarily captured by the target, it has an increased interaction time. This causes additional distortion of the target whose magnitude depends on the lifetime of the resonance. Consequently, the effect of a resonance in enhancing inelastic cross-sections is dependent on the lifetime. For example, long-lived resonances with lifetimes, Δt larger than 10^{-14} seconds cause a significant displacement of the nuclei of a molecule when the additional electron occupies a strongly bonding or antibonding orbital. When the electron leaves the molecule, nuclear motion is initiated toward the initial internuclear distance, causing excitation of many overtones of the molecule, due to the strong overlap between the nuclear wave function of the resonant state and that of many vibrational states of the ground state of the molecule. On the other hand, when Δt is much smaller than a typical vibrational period ($\Delta t << 10^{-14}$ s), the nuclei are not significantly displaced. In this case, overlap between the nuclear wave function of the resonant state and that of the vibrational levels of the ground state occurs only between the first few energy levels. Thus, for short resonance times only the lower vibrational levels become excited with considerable amplitude.

Because of the uncertainty principle (i.e., $\Gamma \cdot \Delta t \approx \hbar$), the transient state has a width in energy Γ which serves to characterize and identify the process in the energy dependence of the scattering cross-sections or excitation functions. Thus, when resonances are short-lived ($\Delta t << 10^{-14}$ s), they produce broad peaks in their decay channels (e.g., in the specific excitation functions where they appear). Long-lived resonances ($\Delta t \geq 10^{-14}$ s) in atoms produce sharp peaks in elastic and electronic excitation and ionization cross-sections. In molecules, they have more decay channels due to the additional degrees of freedom introduced by nuclear motion. Figure 1 illustrates the possible decay channels of a diatomic transient anion AB^-. The departing electron may leave the molecule in a rotationally, vibrationally (process 1 in

Table 3. List of symbols.

d	Film thickness (meter)
e	Unit charge (coulomb)
E_i	Incident electron energy (eV)
E_{k0}	Electron initial energy with momentum $\mathbf{k}_o$ (eV)
E_k	Final electron energy with momentum $\mathbf{k}$ (eV)
h	Planck constant (joule.second)
$\hbar$	$h/2\pi$ (joule.second)
I_0	Primary beam current (ampere)
J_0	Incident current density (ampere/meter^2)
k_0	Electron initial momentum (kg.m/second)
n	Order of polynomial
$N^T(t)$	Number of intact molecules at time t
P_n	Legendre polynomials
Q	Scattering probability per unit length (1/meter)
Q_e	Quadrupole moment (coulomb.meter)
R	Internuclear separation (meter)
r	Distance (meter)
R_e	Equilibrium internuclear separation (meter)
$\hat{r},\hat{R}$	Direction vectors
$S(E_i)$	Surface of constant energy in reciprocal space (meter^{-2})
t	Time (second)
V	Potential (volt)
v	Vibrational quantum number
V_0	Lowest conduction level (eV)
α	Spherically symmetric polarizability (meter$^3/\epsilon_0$)
α'	Non-symmetric part of polarizability (meter$^3/\epsilon_0$)
β	Ratio between mass of ion and parent molecule
Γ	Resonance width (eV)
ΔE	Energy loss (eV)
Δt	Resonance lifetime (second)
Δv	Change of vibrational quantum numbers
ΔV	Charging potential (volt)
ϵ_0	Dielectric constant (coulomb^2/newton.meter^2)
θ_0	Angle of incidence defined from the normal of the surface (radian)
θ_r	Angle at which scattered electrons are measured, defined from the normal of the surface (radian)
$\lambda(E_i)$	Mean free path of electrons of energy E_i (meter)
μ_e	Electric dipole moment (coulomb.meter)
ν	Frequency (hertz)
ρ	Trapping cross-section (meter^2)
σ_D	Effective dissociation cross-section (meter^2)
σ_0	Initial trap density (meter^2)
$\sigma(t)$	Charge density (coulomb/meter^2)
τ	Relaxation time of electron (second)
$\|\chi\rangle$	State of Block electron
$\|\chi_k\rangle$	Final electron state of momentum $\mathbf{k}$
Ω	Volume of crystal (meter^3)

Fig. 1), or electronically (process 2 in Fig. 1) excited state. If the resulting electronically excited neutral state is dissociative, ground state or excited fragments can be produced (2, in Fig. 1). If the lifetime of the resonance is, at least, of the order of a vibrational period, and the AB^- state is dissociative in the Franck-Condon (FC) region, and at least one of the possible fragments has a positive electron affinity, then the anion may dissociate into a stable anion and a neutral fragment in the ground or an excited state (3 and 4 in Fig. 1, respectively). This process is called dissociative electron attachment (DEA). If during its lifetime, the transient anion transfers energy to another system (e.g., by collisional interaction with another molecule, or phonon creation in a surrounding medium), it may stabilize as long as the parent molecule has a positive electron affinity (process 5 in Fig. 1). Finally, when the transient anion is formed at energies above the ionization potential, two-electron emission is also possible (process 6 in Fig. 1). Excluded from the reactions of Figure 1 is the spontaneous emission of a photon by the transitory anion (i.e., $AB^{-*} \rightarrow AB^- + h\nu$), since emission of electromagnetic radiation is rarely faster than electron emission. For further information on the mechanism of transient anion formation and its effects in isolated electron-atom and electron-molecule collisions, see the review articles by Schulz [183, 184] and others [1, 25, 91, 114]. A review of electron resonance scattering from molecules adsorbed in monolayer (ML) or submonolayer amounts on conductive surfaces can be found in the articles by Palmer and Rous [120] and Palmer [119].

When the time-dependent amplitude of the projectile electron wave function does not increase significantly at a particular target site, the scattering process is considered to be direct. In this case, insight into the physical phenomenon may still be gained from analysis of the interaction potential, in trying to determine the leading term (or terms) of its expansion. Consider, as an example, the electrodynamic interaction potential acting between a molecule and an electron outside a molecule [196]. This potential can be written as

$$V = (\mu_e/r^2)\, P_1(\hat{r}\cdot\hat{R}) - (Q_e/r^3)\, P_2(\hat{r}\cdot\hat{R}) - (\alpha e^2/2r^4) - (\alpha' e^2/2r^4)\, P_2(\hat{r}\cdot\hat{R}) - \ldots \quad (1)$$

where r is the distance of the incident electron from the molecule and R is the internuclear separation; μ_e is the electric dipole moment (see Table 3 for symbol definitions). The term containing μ_e is necessarily absent in homonuclear diatomic molecules. The second term, involving Q_e, the quadrupole moment, characterizes the quadrupole interaction. These two terms are the "electrostatic" terms, in that, they pertain to the interaction of

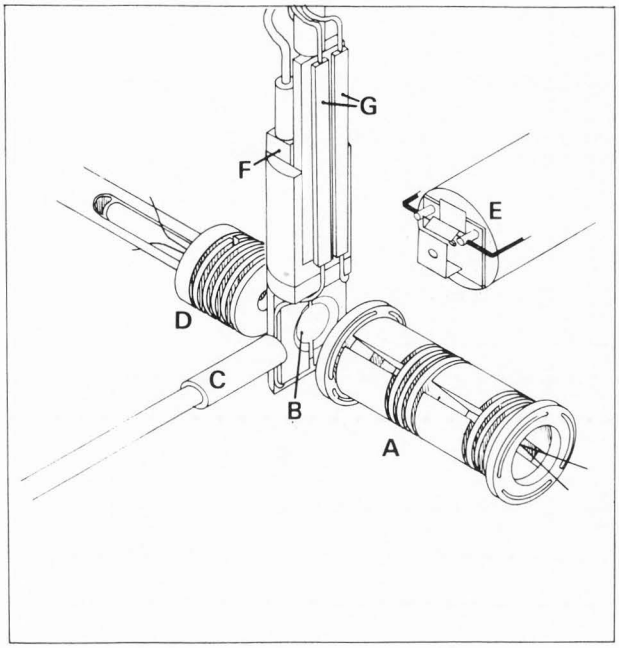

Figure 2. Diagram of typical low-energy electron transmission (LEET) spectrometer with mass spectrometer. A: trochoidal electron monochromator; B: rotatable target; C: gas doser; D: high current electron gun; E: quadrupole mass spectrometer; F: cryostat; and G: electrical leads.

---

the incident electron and the unperturbed molecule. The next two terms, involving α, the spherically symmetric and α', the non-spherical part of the polarizability, are "dynamic" terms. The latter involve the polarization of the molecule by the incident electron. In eq. (1), $\hat{r}$ and $\hat{R}$ are unit vectors in directions r and R, respectively, and P_n are Legendre polynomials. The parameters α, α', μ_e and Q_e are functions of R. It can be seen from eq. (1) that, by estimating the magnitude of the various terms, it may be possible to sort out the dominant scattering mechanism. Furthermore, the potential of eq. (1) can be expanded around the equilibrium internuclear distance R_e as

$$V = V(R - R_e) + (R + R_e)(\partial V/\partial R)\Big|_{R=R_e} + \ldots \quad (2)$$

When only these two terms are considered and the molecule is assumed to be an harmonic oscillator; solving the problem within the Born approximation (usually corresponding to small momentum transfer) leads to the optical selection rule $\Delta v = 1$ for vibrational transitions [66]. Thus, within this most restrictive approximation, the electron behaves like electromagnetic radiation. From this analysis, we can expect the electron-molecule potential described by eq. (2) to be responsible for the magnitude of the differential scattering cross-sections which are large only for small scattering angles and the excitation of the first vibrational energy level ($v = 1$) from the ground state of the molecule.

III. Experiments

The interaction of low-energy electrons within atomic and molecular solids and near their surfaces can be investigated by allowing monoenergetic electrons to impinge on a thin multilayer film grown in an ultra-high vacuum system by the condensation of gases or organic vapors onto a clean metal substrate held at cryogenic temperatures (variable from 15 to 100K in the experiments described here). Depending on the type of experiment, it is possible to measure the incident electron energy dependence of the current transmitted through [160, 177], trapped in [89], or reflected from [131, 170] the condensed film, or of the positive ion [198], negative ion [163], and metastable species fluxes [80] emanating from its surface. As a general rule, the film thickness must be larger than the total electron mean free path if we want to minimize effects of the metal substrate. Small amounts of molecules can be added to the film surface or mixed within the dielectric film to study the effects of dopants. Electron interactions at the interface between two dielectric materials can be studied by covering a given film with an overlayer of another substance. These different types of experiments are briefly described in this section.

IIIa. Low-energy electron transmission (LEET) spectroscopy

A drawing of the type of apparatus used to record LEET spectra [160, 177] and electron stimulated desorption (ESD) yields [163, 198] is shown in Figure 2. It consists of a high current electron gun (D), a quadrupole mass spectrometer (E), a gas introduction doser (C), a cooled target (B), and a high-resolution trochoidal electron monochromator (A). Depending on the instrument, it may be possible to rotate the target (B) and cool it down to 15K with the cryostat (F). All components shown in Figure 2 are housed in an ultra-high-vacuum system reaching pressures $\sim 10^{-8}$ Pa. The magnetically collimated electron beam, leaving the monochromator (A) with a resolution of about 40 meV full width at half maximum (FWHM), impinges on the film condensed onto a metal substrate (B) (i.e., the electron collector). The latter is electrically isolated from the cryostat by a sapphire disk and connected to electrical leads (G). LEET spectra are obtained by measuring the current I_t arriving at the metal substrate as a function of incident electron energy. In these experiments, I_t is of the order of $\sim$ 1 nA and the absolute electron energy scale is calibrated to within $\pm$ 0.15 eV of the vacuum level by

measuring the onset of electron transmission through the films. The metal substrate is usually a polycrystalline metal sheet which can be cleaned by resistive heating via G. The condensed films are grown using a gas-volume expansion dosing procedure [160] which can be calibrated by monitoring the quantum size effect features observed for ultra thin films [124]. With this calibration, the film thicknesses of 1 to 50 nm can usually be estimated with an accuracy $\leq 30\%$ assuming a layer-by-layer growth.

IIIb. Charge trapping

With LEET spectroscopy, it is also possible to measure the number of charges accumulated near the surface of a dielectric film resulting from the electron bombardment [89]. When electrons from monochromator (A) (Figure 2) have just enough energy to enter a multilayer film deposited on the substrate B, a sharp rise, named the "injection curve" (IC), is seen in the LEET spectrum. The IC for an uncharged film is represented by the upper curve of Figure 3. When the same film is charged at the surface by the electron beam, the IC is shifted by ΔV to a higher accelerating potential (bottom curve, Fig. 3), since the incoming electrons must then possess additional kinetic energy (KE) to overcome the negative potential barrier. The IC is also broadened due to the effect of space charge and current density distributions. Such measurements are usually performed in conjunction with all types of thin film low-energy electron experiments to ascertain that the target does not charge significantly during the time of the experiment. However, if the film is purposely allowed to charge at its surface by a significant potential ΔV, this latter can be related to the trapping cross-section, by treating the dielectric film as a charged capacitor [89]. The potential barrier ΔV is related to the charge density $\sigma(t)$, which has accumulated after bombardment time t, by the equations

$$\Delta V(t) = \sigma(t)\ (d/\epsilon);\ \text{and}$$

$$\sigma(t) = \sigma_0\ \{1 - \exp(\beta t)\};\ \beta = (\rho J_0/e) \qquad (3)$$

where, ϵ is the permittivity of the film, d its thickness, σ_0 the initial ($t = 0$) trap density, ρ the trapping cross-section, J_0 the incident current density and e the unit charge. In the limit $t \rightarrow 0$, a charging coefficient $A_s = d\Delta V/dt$, directly proportional to the trapping cross-section, can be expressed as

$$d\Delta V/dt|_{t=0} = \{(d\sigma_0 J_0)/\epsilon e\}\ \rho = A_s \qquad (4)$$

The experiment is performed as follows. The IC of a freshly deposited multilayer film is first recorded rapidly (e.g., during 0.1 s) to avoid any significant charging. The film is then bombarded at a given voltage V

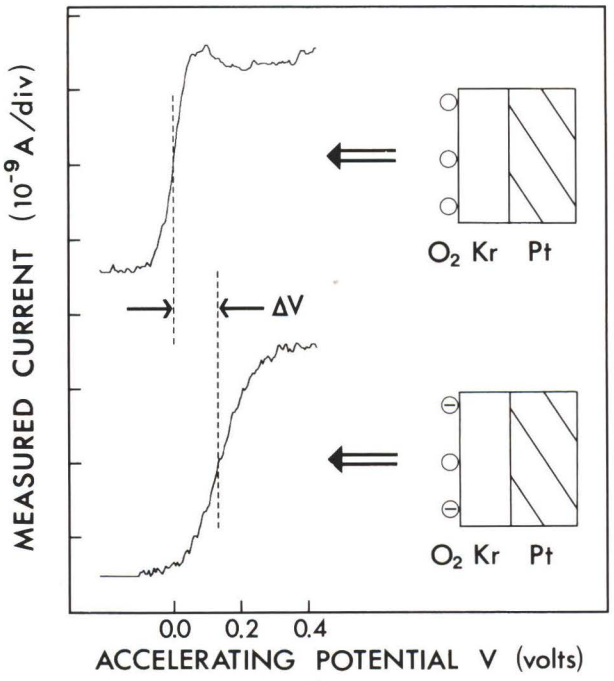

Figure 3. Current transmitted through an uncharged (top) and a charged (bottom) Kr film covered with 0.1 monolayer (ML) of O_2 as a function of the accelerating potential V of the incident electron beam.

---

applied between the monochromator and the film for a much longer period (e.g., 25 s) with the same incident current (i.e., $I_0 \simeq 5 \times 10^{-9}$ A). Afterwards, the IC is again rapidly recorded and the shift ΔV determined by comparison with the initial IC. Such a cycle can be repeated many times on the same film with the same V to obtain the time dependence of the process. To measure the thickness and electron energy dependence, a new film has to be deposited for each data point. However, if film charging can be reduced to the beam resolution, measurements, as a function of electron energy, can be performed on a single film without affecting considerably the total energy resolution of the experiment (to be published).

IIIc. Electron stimulated desorption (ESD) of ions

A portion of the positive and negative ions produced by electron impact on the film target B (Fig. 2) can be measured by placing a mass spectrometer (E) near the film surface [7]. In the experimental arrangement of Figure 2, the cryostat is rotated toward E for this measurement. Ions emerging from the film are focused by lenses located in front of the entrance of the mass spectrometer. Grids can be inserted between the lenses and the mass spectrometer in order to analyse the ion energies by the retarding potential method. The apparatus can be operated in two modes [7]: the ion-yield mode in

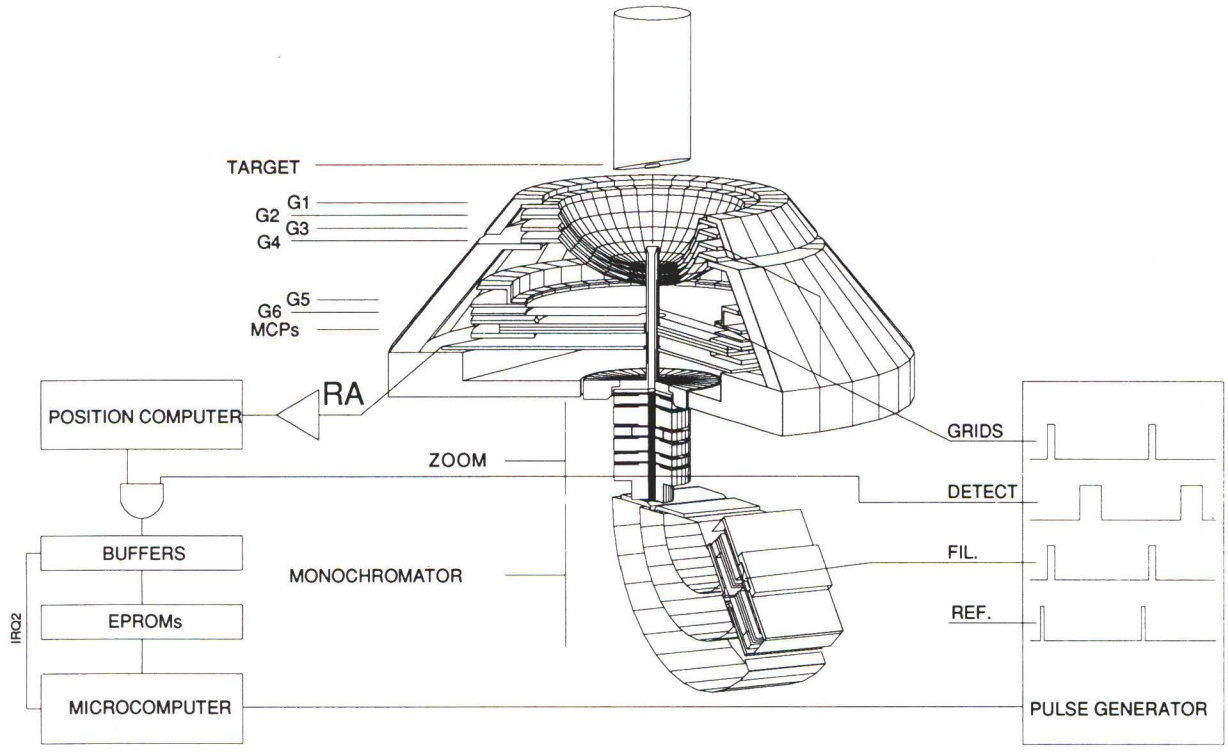

Figure 4. Schematic view of the apparatus used to measure the angular distribution and time of flight of particles desorbed by electron impact. It includes the electron source, the grids, the target, the detection system, the associated electronics, and the pulse sequence applied to the various components.

---

which ions of a selected mass are detected as a function of incident electron energy, and the ion-energy mode in which the ion current at a selected mass is measured for a fixed electron energy as a function of the retarding potential.

IIId. Ultra-violet (UV) luminescence and metastable desorption

In more sophisticated systems, it is also possible to measure the angular distributions of UV radiation emitted and metastable species and ions desorbed by electron impact [80, 81]. An apparatus of this type [81] is described in Figure 4; in it, a monoenergetic electron beam, emanating from an electrostatic monochromator, is incident on a solid target. Charged particles can be discriminated or energy analyzed by a set of 4 grids (G1-G4) before they enter a field-free region between grids G4 and G5. They are subsequently accelerated onto an imaging device consisting of a stack of three gold-coated microchannel plates (75 mm diameter detecting area) mounted above a resistive anode. The latter is coupled to a pulse counting position computer. The image coordinates are digitized, buffered, distortion corrected in real time, and stored in a microcomputer. This storage can be time discriminated following an incident electron pulse so as to perform two-dimensional time-of-flight (TOF) analysis. The analysis for metastable species and UV photons is obtained with large positive and negative potentials on grids G2 and G3 respectively, in order to repel all charged particles. With these potentials, the space integrated TOF spectra consist of a sharp photon signal followed by others corresponding to metastable species of different energies and/or masses. Allowing negative charges to pass through the grids superimposes the contribution from electrons and anions. In the negative charge counting mode, the bidimensional image at short time corresponds to electrons and those at long times to anions. On single crystals, the electrons produce LEED patterns.

IIIe. High resolution electron energy loss (HREEL) spectroscopy and excitation functions

Energy losses by electrons scattered near the surface of thin films and their energy dependences are measured with a HREEL spectrometer [170]. The experimental assembly is similar to the one shown in Figure 2, where component A and E are replaced by two hemispherical electrostatic deflectors. One of them produces a focused monochromatic electron beam, striking the surface at an angle θ_0 from the film normal. The other analyzes the energy of electrons scattered outside the target at an angle θ_r from the film normal. Depending on the type of

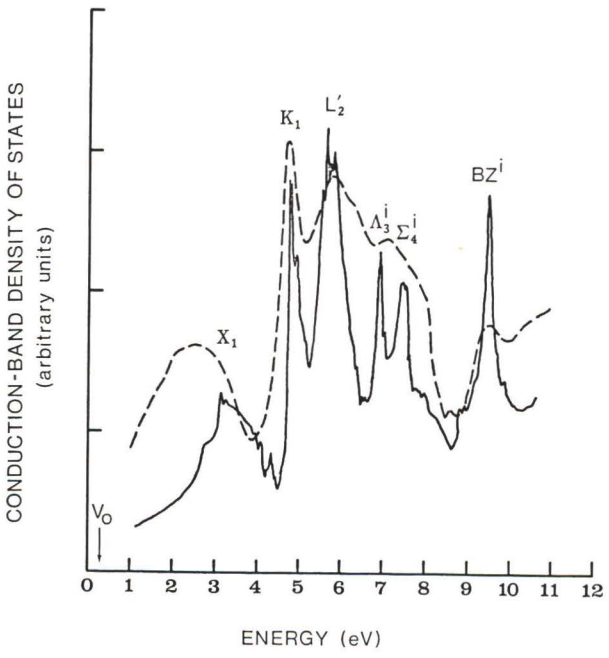

Figure 5. Electron conduction-band density of states of solid argon [133]: calculated (full line) and determined from analysis of LEET data for solid argon recorded at ~ 20K. The zero of energy is that of the vacuum level. V_o is the energy of the bottom of the conduction band.

HREEL spectrometer, the angles θ_0, θ_r or both can be varied within limits set by the physical arrangement. Energy-loss spectra are recorded by sweeping the potential of either the monochromator or the analyzer with respect to the grounded target. The energy dependence of the magnitude of a given energy loss event (i.e., the excitation function) is obtained by sweeping the energy of both deflectors with a potential difference between them, corresponding to the probed energy loss.

IIIf. Dissociation cross-sections

To directly measure radiation damage caused by the impact of slow electrons, a high current electron gun (D, in Fig. 2) is used to degrade the film [79]. The beam current produced by this electron gun ($I_0 \approx 5 \times 10^{-5}$ A) is collimated by an axial magnetic field of 10 gauss but strongly defocused by the lens system to obtain an area of about 0.4 cm^2 at the target surface. Near-zero incident energy is attainable within an energy resolution of 450 meV FWHM. The absolute value of the film thickness can be obtained from LEET spectra recorded with the monochromator. Then, the energies of the structures appearing in LEET spectra are correlated with those appearing in the transmitted current versus energy curves obtained with the high-intensity electron beam (i.e., from gun D) to establish the absolute energy scale of the latter.

After bombardment for a time t with the radially symmetric electron density $J_0(r)$ from gun D (Fig. 2), the target is heated to sublime the film near the entrance of a mass spectrometer (E, Fig. 2) tuned on the mass of the condensed molecule. The integrated mass peak signal is proportional to the number of molecules $N^T(t)$ which remain intact during bombardment. $N^T(t)$ is a sum of decreasing exponentials of the form exp $\{-\sigma_D J_0(r)t/e\}$ which defines [79] the effective dissociation cross-section σ_D. $J_0(r)$ is the spatial electron current density. By measuring J_0 independently, σ_D can be obtained from $N^T(t)$.

IV. Elastic and Quasi-Elastic Scattering

Elastic and quasi-elastic scattering of low-energy electrons by multilayer rare gas and molecular solid films has been investigated by LEET spectroscopy [14, 15, 21, 24, 39, 40, 41, 42, 45, 49, 51, 56, 57, 59, 69, 72, 73, 104, 113, 123, 124, 125, 132, 133, 134, 160, 177, 178, 179, 199, 200], photoinjection [18, 22, 23, 90, 127] and elastic reflection [101, 104, 105, 107] experiments. In the latter, a HREEL spectrometer is adjusted to measure electrons elastically scattered from a film at particular incident and scattered angles θ_0 and θ_r. Then, the amplitude of the elastic peak is measured as a function of incident electron energy. Since in these experiments, both the incident and outgoing electron momenta are specified, features due to interferences of the electron waves are prominent in the spectra. In well-ordered films, the diffraction structure is dominated by long-range order [104], whereas in amorphous substances, variation in the structure factor, due to short-range order, can be detected in the energy-dependence of the elastic reflectivity [101].

Both LEET and photoinjection experiments, measure the electron current transmitted through a multilayer film deposited on a metal substrate. In the photoinjection experiment [90], electrons are injected in the film from the metal substrate with ill-defined energies and momenta, but the outgoing electrons which escape into the vacuum at a given energy and momentum can be selected with an electron analyzer.

In transmission, only the incident beam has a well-defined energy and momentum, since current which has been scattered into all angles is measured at the metal substrate. Furthermore, when the film is highly disordered, electrons are scattered in all possible directions near the surface [15], so that the penetrating momentum is also unspecified. **This condition closely resembles that found in electron microscopy where secondary electrons bear no phase, momentum and energy relationship with each other and are therefore highly incoherent.** Furthermore, because of their short mean free paths, they quickly start losing energy to phonons

of the solid so that pure elastic scattering does not occur to any substantial extent.

Electron scattering which results in multiple energy losses to phonons is expected to depend on the electron conduction band density of states (CDOS) and the electron-phonon interaction. The calculated CDOS of solid Ar (solid line) and that extracted from LEET spectra [133] of multilayer (20-100 ML) Ar films (dashed line) are compared in Figure 5. There exists an obvious relationship between the two sets of data which indicates that it is essentially the CDOS which governs quasi-elastic scattering of the low-energy electrons. In a recent analysis of HREEL experiments [43], it has been shown that this correspondence arises because of multiple energy losses to phonons by the scattered electrons. Taking again the example of an Ar multilayer film, this relationship is shown in Figure 6; the curves in the figure were recorded with a HREEL spectrometer set to measure the dependence on incident electron energy of the energy loss $\Delta E = 0.25$ eV at several incidence angles between 15° and 65°. Therefore, these curves represent the probability for an electron, penetrating a 50-layer film of Ar deposited on Pt, to lose 0.25 eV via multiple losses to phonons in the solid. Except for the measurement at $\theta_0 = 45°$ (i.e., in the specular direction), all the features are found essentially at the same energy, independently of the incident angle. The similarity between these curves reveals an electron-scattering property of the solid that is averaged over various directions of electron propagation (i.e., various electron states) which may consequently reflect the CDOS. In Figure 6b, the CDOS of Ar as calculated by Bacalis *et al.* [13], is displayed with the bottom of the lowest conduction band fixed at the measured value [199] of 0.25 eV above the vacuum level. As one can see, the experimental curves of Figure 6a, and especially those for large incident angles, show a close resemblance with the CDOS. The closer agreement at large θ_0 presumably arises from a better averaging over the incident direction due to the disordered arrangement of the deposited polycrystalline films. With the exception of the peaks around 9 and 12 eV, all the calculated features appear progressively shifted to higher energies, with respect to the experiment, by ~ 0.25 eV at low energies to ~ 1 eV at the highest energy. In this regard, it should be noted that the calculations have been performed with a face centered cubic lattice parameter of 0.526 nm, while a larger value of 0.531 nm (typical of solid Ar between 4 and 20 K) [126] would have yielded a more compact density of states [137, 138] and consequently an overall better agreement.

One can explain the similarity between the experimental results and the calculated CDOS by focusing on the electron transport properties in the bulk [105, 107].

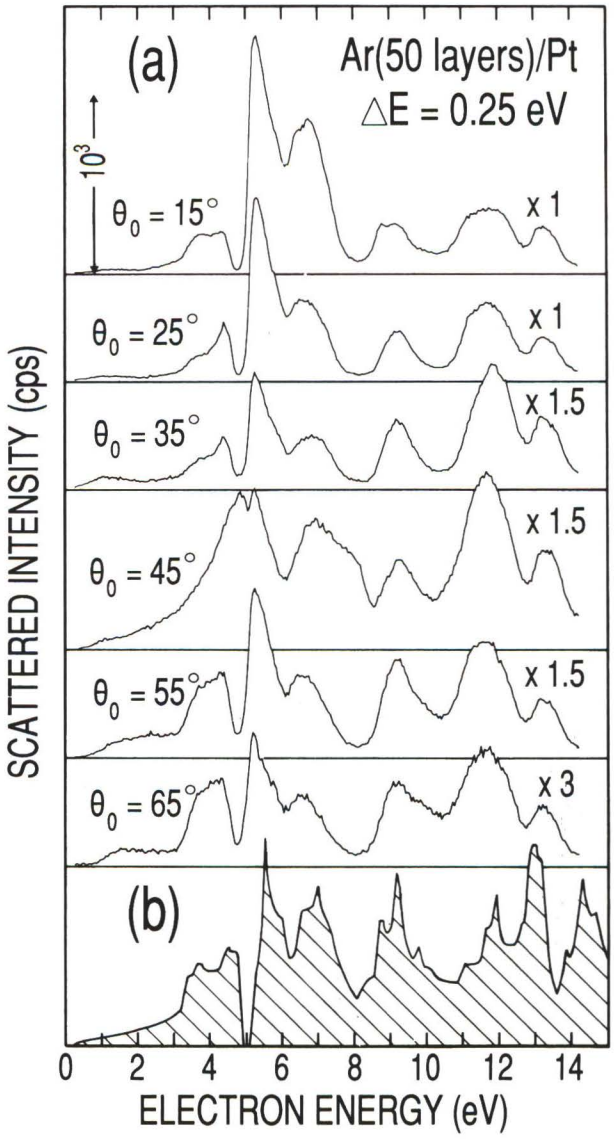

Figure 6. (a) Scattered electron intensity at the fixed energy loss of $\Delta E = 0.25$ eV as a function of the incident electron energy for several angles of incidence θ_0 on a fifty-layer film of Ar. (b) Conduction-band density of states for the fcc structure of solid Ar as calculated by Bacalis *et al.* [13].

An electron propagating in a conduction band of a rare gas solid suffers scattering mainly from defects and lattice waves. This can be described by introducing the scattering probability per unit length $Q(E_{k0}, \mathbf{k}_0, E_k, \mathbf{k})$ that a Bloch electron initially in a state $|\chi\rangle$ of momentum $\mathbf{k}_0$ and energy E_{k0} is scattered into a final state $|\chi_k\rangle$ of momentum $\mathbf{k}$ and energy E_k, while the crystal changes from a state $|i\rangle$ of energy ϵ_i to a state $|f\rangle$ of energy ϵ_f. Then, by referring to the "golden rule" and

solving the Boltzmann transport equation for a plane-parallel system in the "two-stream" approximation [14, 98, 101], one obtains for the electron mean free path $\lambda(E_i)$ (i.e., the reciprocal of Q) the expression

$$\lambda(E_i) \equiv \langle \{ \sum_{\mathbf{k}} Q(E_{\mathbf{k}0}, \mathbf{k}_0, E_{\mathbf{k}}, \mathbf{k}) \}^{-1} \rangle_{E_i} \qquad (5)$$

where E_i is the incident electron energy.

In this expression the **k** summation extends over the first Brillouin zone, whereas $\langle \ldots \rangle$ stands for the average over the incident direction $\mathbf{k}_0$ for a constant incident energy $E_{\mathbf{k}0} = E_i$. If we replace the summations with integrations and assume for simplicity that the matrix element for calculating Q depends only on the momentum transfer (i.e., $|\mathbf{k} - \mathbf{k}_0|$), eq. (5) yields

$$\lambda(E_i)^{-1} = D(E_i) \langle \{8\pi\hbar/\Omega S(E_i)\} \{1/\tau(E_i)\} \rangle \qquad (6)$$

where $D(E_i)$ is the CDOS of the solid at the energy E_i, $\tau(E_i)$ corresponds to a relaxation time (i.e., the time between scattering events) independent of the $\mathbf{k}_0$ direction, $S(E_i)$ is the surface of constant energy E_i within the first Brillouin zone, and Ω is the volume of the crystal. Within the approximations of an electron effective mass and of an electron-phonon interaction described as a deformation-potential perturbation, one has [75] $1/\tau(E_i) \propto |\mathbf{k}_0|^2$ and $S(E_i) \propto |\mathbf{k}_0|^2$. Consequently, the expression in parentheses in eq. (6) is independent of E_i and the energy dependence of $\lambda(E_i)^{-1}$ or Q (i.e., the quasi-elastic scattering probability per unit length) becomes directly proportional to the CDOS as shown experimentally in Figure 6.

The example of Figure 7 shows how the CDOS features in a LEET spectrum (unpublished) reflect changes in the geometrical arrangement of the molecules of a n-hexane film. The LEET spectra in Figure 7 were recorded for a five ML n-hexane film condensed and held at the temperatures specified in the figure. The broad peak centered around 11 eV is due to energy-loss electrons having produced electronic excitations. Below 8 eV, only elastic and quasi-elastic scattering is possible and therefore, the LEET features reflect structure in the CDOS. As seen from Figure 7, these features are temperature dependent, indicating that above 60K a crystalline state of the solid starts to form. LEET spectra recorded at 70K and above do not exhibit significant changes. Hence, at 70K, the crystalline state appears to be well established; below 40K, a more disordered or amorphous state predominates. Since the band-gap edge (i.e., the lowest conduction level V_0) of n-hexane lies **0.8 eV above the vacuum level**, the sharp peak near 0 eV is due to electron conduction in gap states as shown by Caron *et al.* [21].

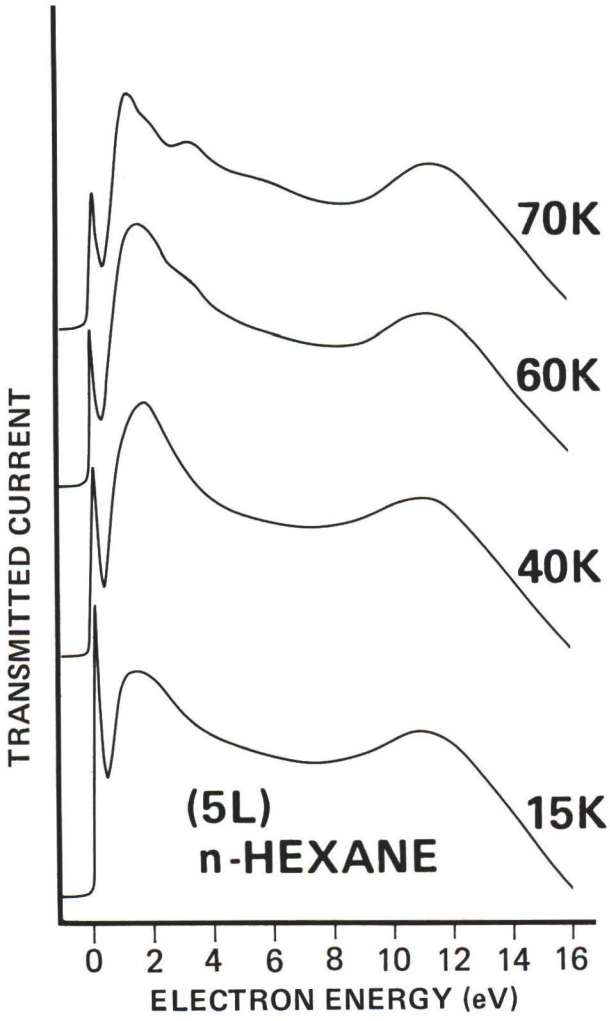

Figure 7. LEET spectra of a 5 ML film of n-hexane recorded at different temperatures.

V. Vibrational Excitation

By scattering within atomic and molecular solids and at their surfaces low-energy electrons can excite, with considerable cross-sections, not only phonon modes of the lattice [26, 43, 99, 100, 101, 105, 107, 108, 109, 170] but also individual vibrational levels of the molecular constituents of the solid. Excitation of these modes has been investigated by HREEL spectroscopy both at fixed incident energies and as a function of incident electron energy [2, 3, 16, 20, 26, 30, 36, 47, 58, 67, 68, 88, 93, 99, 100, 101, 102, 110, 111, 129, 130, 131, 139, 140, 141, 142, 144, 154, 167, 168, 169, 170, 171, 172, 179, 182, 195, 197, 201, 202]. These modes can be excited either by direct or by resonant scattering conditions which prevail at specific energies; as shown in this section, resonances can enhance this energy-loss process by orders of magnitude.

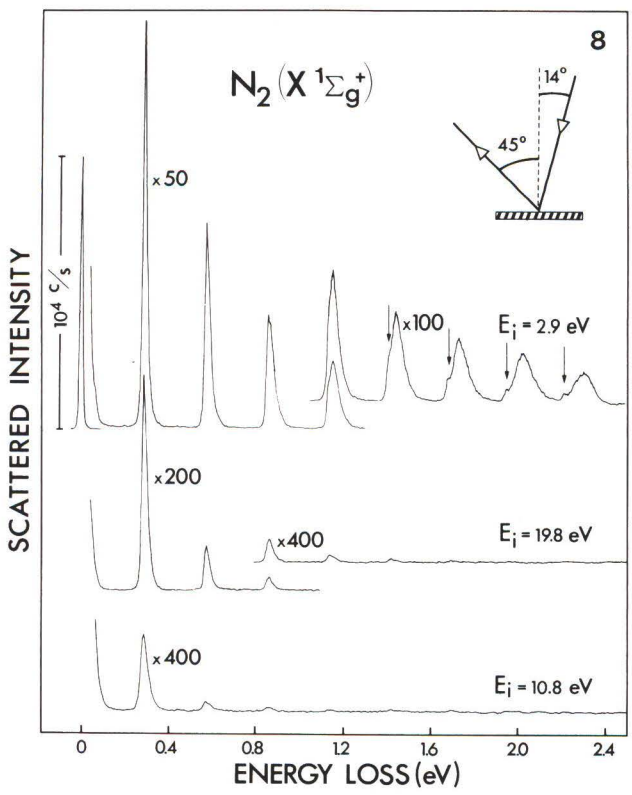

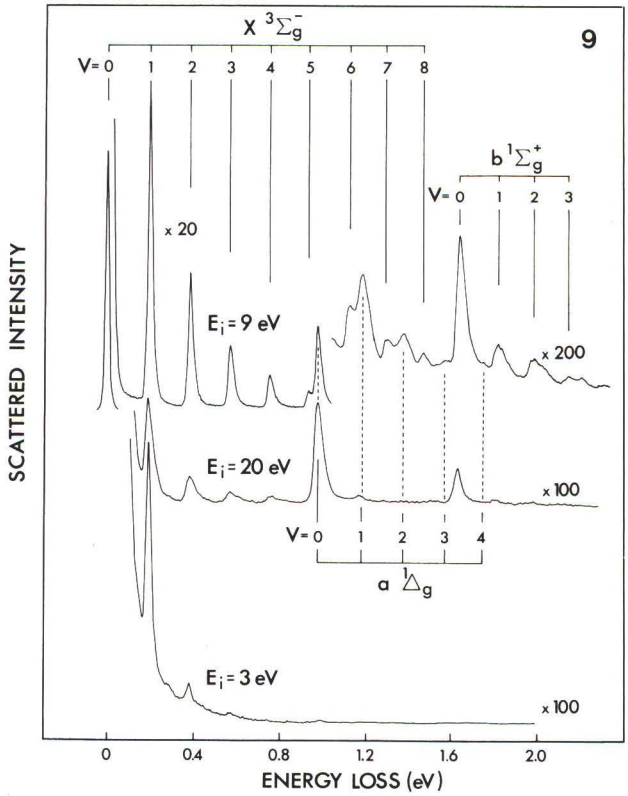

Figure 8 (at left). High-resolution electron-energy-loss (HREEL) spectra of a multilayer disordered N_2 film [167] recorded at primary energies of 2.9, 19.8 and 10.8 eV. The intensity of the elastic peak is indicated in counts/second (c/s). The enhancement in vibrational excitation of ground-state N_2 at 2.9 and 19.8 eV results from the formation of temporary negatively charged states of N_2 in the solid.

Figure 9 (at right). HREEL spectra for electrons of primary energies E_i = 9, 20 and 3 eV incident at $\theta_0 = 14°$ on a multilayer disordered O_2 film.

Va. HREEL spectra

Examples of excitations of the vibrational modes of ground state N_2 and O_2 within 5 nm multilayer films of these molecular solids are shown in Figures 8 and 9, respectively. These electron energy loss spectra were recorded for electrons of energies E_i = 3, 9, and 20 eV in O_2, and E_i = 2.9, 10.8 and 19.8 eV in N_2. In all experiments, $\theta_0 = 14°$ and $\theta_r = 45°$. The vertical gains in each curve or portion of a curve are referenced to the elastic peak. Each energy-loss peak in Figure 8 can be ascribed to vibrational excitation of ground state N_2 [167]. Additionally, in O_2 films [168], some vibrational progressions can be ascribed to intramolecular vibrational excitation of the states $a^1\Delta_g$ and $b^1\Sigma_g^+$ (Fig. 9). It can be seen that at certain impact energies (E_i = 2.9 eV and 19.8 eV for N_2, and 9 and 20 eV for O_2, respectively), the intensities of vibrational energy losses are greatly increased (i.e., up to two orders of magnitude for overtones). In N_2 films, production of overtones at E_i = 2.9 and 19.8 eV is attributable to $^2\Pi_g$ and $^2\Sigma_u^+$ shape resonances [167]. Similarly, in the energy loss spectra of multilayer O_2 films (Fig. 9), the strong enhancement in vibrational excitation of O_2 in the configuration $^3\Sigma_g^-$ has been interpreted as due to the formation of two overlapping transient anions [168]: the $^2\Pi_u$ and $^4\Sigma_u^-$ states of O_2^-. Only the $^2\Pi_u$ anion decays to the $^1\Delta_g$ and $^1\Sigma_g^+$ states due to spin conservation.

There are no electron resonances at E_i = 10.8 eV in N_2 and 3 eV in O_2. In these cases, the strongest part of the interaction leading to vibrational excitation arises mainly from induced polarization {i.e., from direct scattering, via eqs. (1) and (2)}. This interaction is mainly effective to produce excitation of one vibrational quantum which amounts to an energy loss of less than 0.4 eV for N_2 and O_2.

Vb. Excitation functions

Modification of a gas-phase resonance by the condensed phase, as observed by its decay into vibrational excitation, is illustrated in Figure 10. The lowest curve (Fig. 10) is the excitation function for v = 1 vibrational excitation of gaseous N_2 in the ground state. The other

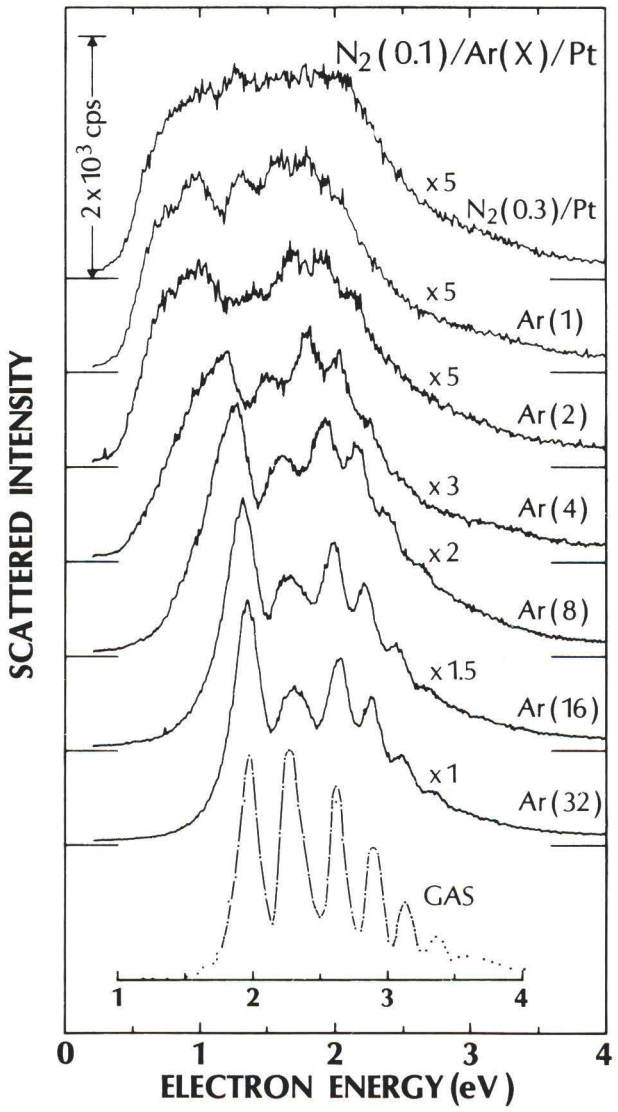

Figure 10. Excitation function for the v = 1 level of N_2 when separated from the Pt substrate by an Ar film of thicknesses ranging from 0 to 32 layers. The angle of incidence $\theta_o = 14°$ and that of analysis $\theta_r = 45°$. The N_2 coverage is 0.1 layers for all Ar thicknesses except it is 0.3 layers at 0 layer of Ar. At the bottom, the corresponding differential cross-section measured in the gas phase is shown, aligned with the 32-layer result.

---

curves are the same function obtained with 10% surface coverage of N_2 deposited on an Ar multilayer film of variable thickness (i.e., from 0 to 32 ML as denoted in the parentheses on the right of Fig. 10). The 32 ML result indicates that only with a small amount of N_2 on the surface, a significant amount of electron energy, in the range 1 to 3 eV, is transformed to vibrational excitation of ground state N_2. The oscillatory structure, which modulates the broad peak in each excitation function of Figure 9, results from vibrational motion of the $^2\Pi_g$ transient N_2^- state [169]. The average spacing between the first six of these vibrational peaks is 0.27 eV for the gas-phase data as compared to the corresponding value of 0.29 eV in the solid [169]. Once appropriately translated by -0.62 eV all peak positions of the gas-phase measurement agree within ± 0.02 eV with those of the 32-layer result. This lowering of the energy of the $^2\Pi_g$ anion is due to electronic polarization of the Ar surface by the temporarily localized charge.

If the lifetime of the anion were long compared with one vibrational period of a N_2 molecule, the oscillatory structure in Figure 10 would form non-overlapping, well-defined peaks corresponding to vibrational levels of N_2^-. On the other hand, if the lifetime were much shorter than a vibrational period, no structure at all would be observed. In the intermediate case (i.e., lifetime of the order of the vibrational period), overlapping oscillatory structure is observed. Thus, the structure in Figure 10 does not truly represent vibrational levels but indicates that the lifetime of the resonance is of the order of a vibrational period of N_2 ($\simeq 10^{-14}$ s).

The results of Figure 10 further illustrate the effects of the metal substrate on the $^2\Pi_g$ resonance which is shown by varying the N_2-metal distance from experiments with the various Ar layer thicknesses. For film thicknesses smaller than 32 ML, the overall intensity of the broad resonance feature decreases considerably, while the oscillatory structure shifts to lower energy and becomes broader. However, the relative separation between the peaks appears to be almost unperturbed. The increased broadening of the peaks can be attributed partly to fluctuations in the surface potential near the metal surface and to a reduction in the lifetime of the N_2^- state with increasing proximity to the metal [102]. Furthermore, the reduction of the intensity with diminishing thickness can also be attributed to a decrease of the resonance lifetime. Considering that the inelastically scattered intensity for pure N_2 on Pt was recorded at 0.3 ML coverage, we find a decrease of a factor of 15 in the energy losses to vibrational excitation at the metal surface. This result indicates that energy losses by low-energy and secondary electrons to such energy modes are likely to be significantly decreased near metal surfaces when transient anions (i.e., resonance processes) control the vibrational excitation cross-sections. Since this is generally the case for molecular and organic solids, **changes in specimen damage during electron spectroscopy and microscopy measurements are expected near metal surfaces (e.g., near the substrate surface).**

This method of investigation can also be applied to study the behavior of slow electrons within the bulk of molecular solids. The HREEL spectra of N_2 (Fig. 8) and O_2 (Fig. 9) solids represent energy losses from both

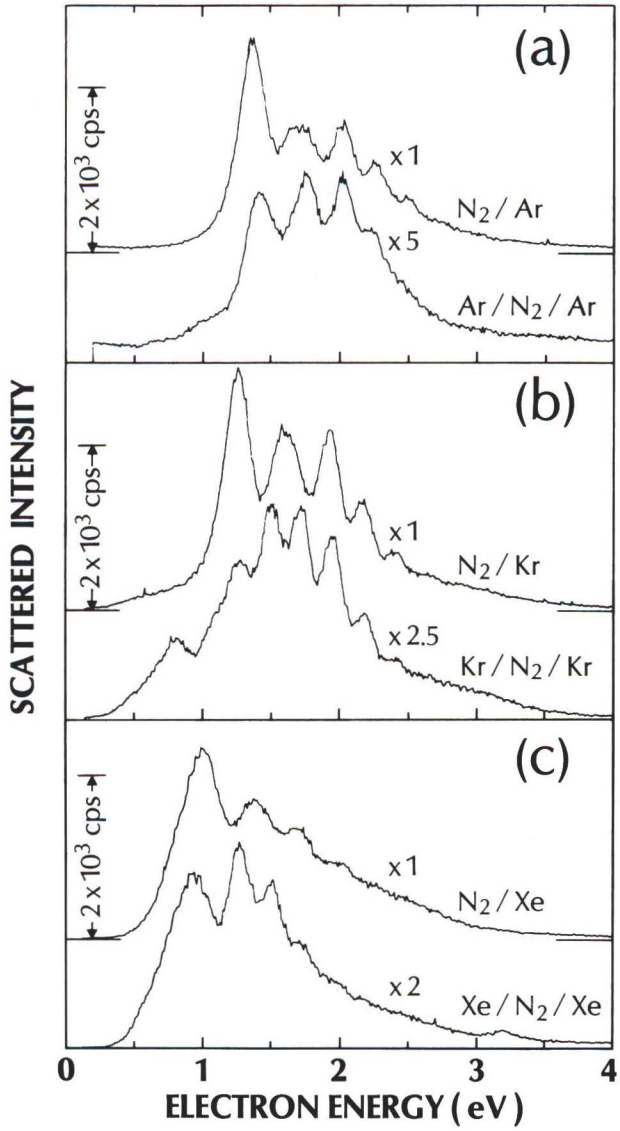

Figure 11. Excitation function for the v = 1 level of N_2 deposited on the surface of a 32-layer rare gas film and on a 16-layer rare gas film with an additional 16-ad-layer of the same rare gas is shown for Ar (a), Kr (b) and Xe (c).

---

the surface and bulk of the films. However, the effect of the bulk of the solid and band structure on a specific vibrational excitation cross-section of a particular molecule can be best identified by measuring its excitation function within a solid film containing the probed molecule. Figure 11 shows again the excitation function of the v = 1 level of N_2 within the 0-4 eV range, but this time, for a 0.1 ML quantity of N_2 embedded within (a) Ar, (b) Kr, and (c) Xe 32 ML films [106]. Each portion of Figure 11 also exhibits the excitation function for the v = 1 level of N_2 deposited on the surface of a 32 ML rare gas film. It may be seen that both the energy

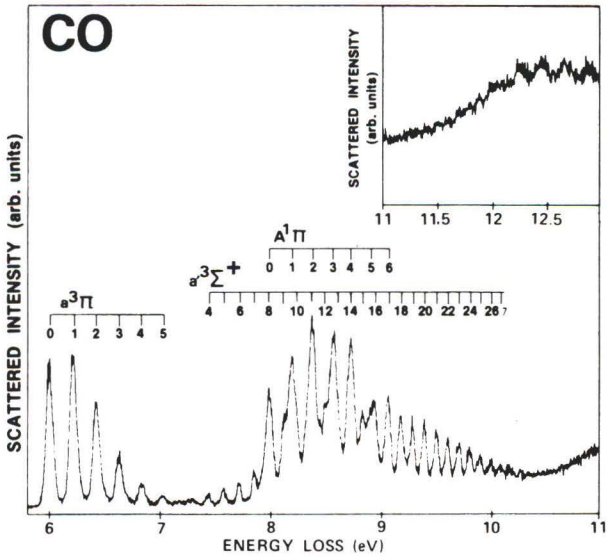

Figure 12. HREEL spectrum of CO condensed on Pt in the energy-loss range 5.9-13 eV. The incident energy is 19 eV; $\theta_o = \theta_r = 45°$.

---

and line shape of the $^2\Pi_g$ state are dependent on the nature of the substrate and coverage by additional RG solid layers. The energy-integrated magnitude of the resonant phenomena is practically the same for all cases but the relative magnitude of each peak in the oscillatory structure may differ considerably. One notices that the lowest energy peak in the surface spectra of Ar and Kr has a smaller amplitude in the excitation functions for N_2 embedded in RG solids; it is also shifted down by 0.27 and 0.43 eV, respectively, due to the increased electronic polarization within the solid. For bulk Xe, the lowest energy peak is no longer visible in the excitation function (Fig. 11c).

VI. Electronic Excitation

Non-dissociative electronic excitation by low-energy electrons in multilayer atomic and molecular films has been investigated by LEET [5, 14, 40, 41, 52, 53, 54, 55, 78, 87, 88, 160, 177, 178, 187] and HREEL spectroscopies [6, 19, 88, 97, 103, 106, 111, 116, 143, 166, 168, 171, 190, 191, 192, 193, 194] and, more recently, by ESD and UV detection techniques [4, 80, 81, 84, 85, 86]. The excitation of electronic states of atoms and non-dissociative electronic states of molecules in dielectrics can result in localized energy depositions [166, 193] or into the formation of excitons [103] moving within the solid with a well-defined wave vector. In the following two subsections, we provide examples of these major classes of electronic excitations in atomic, molecular and organic solids. The first class is illustrated with the HREEL spectra of CO, butadiene and cyclopentadiene films; the second with desorption caused by electronic excitations induced in rare gas solid films.

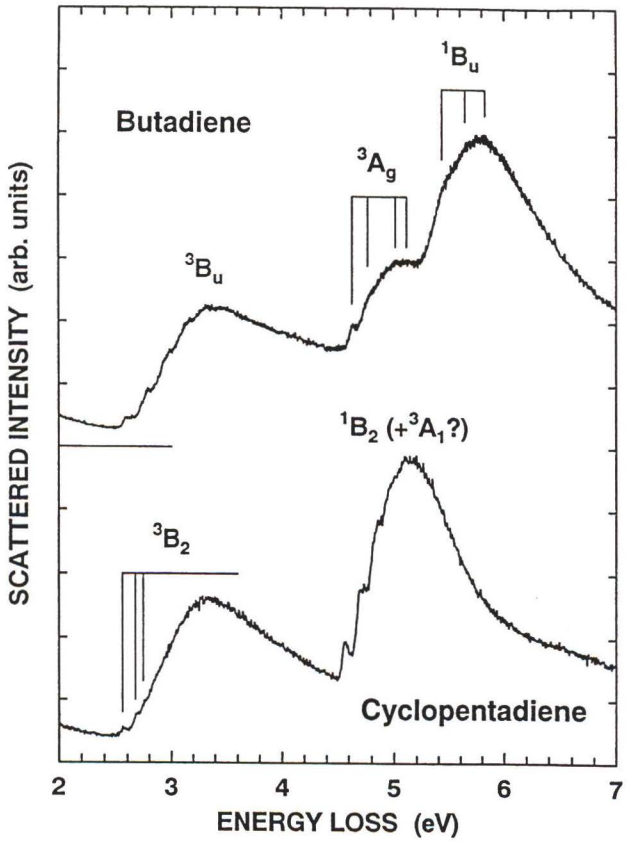

Figure 13. Electron-energy-loss spectra of butadiene and cyclopentadiene condensed on ten-layer argon films recorded at $\theta_o = 14°$, $\theta_r = 45°$ and $E_i = 9.5$ eV. The thickness of the butadiene films corresponds to a monolayer coverage, whereas cyclopentadiene films are at least twice as thick.

VIa. HREEL spectra

Figure 12 displays HREEL spectra [88] for 15 ML of CO on Pt recorded at 19 eV incident energy and $\theta_i = \theta_r = 45°$. The intensities of energy-loss peaks are about three orders of magnitude smaller than the elastic ones. Below 10.5 eV, these spectra are similar to those recorded in the gas phase at the same primary energy and at $\sim 90°$ from the primary beam [29]. Above 10.5 eV (inset Fig. 12), in a region where an abundance of Rydberg states appears in the gas phase, only a few weak peaks are seen.

The data in Figure 12 indicate that the positions of all the peaks are shifted down by $\sim$ 30 meV with respect to the gas-phase values [29, 50]. The shift is more important ($>$ 25 meV) for high values of the vibrational quantum number. The energy resolution of the electron beam allows the detection of broadening of the energy levels whose actual width can be estimated easily if we assume that the observed FWHM results from the convolution of two Gaussian line shapes. For well-resolved vibronic peaks in CO, the estimated FWHM is 30, 14, and 31 meV for the $a^3\Pi$, $a'^3\Sigma^+$, and $A^1\Pi$ states, respectively [88]. Peak broadening can result from multiple scattering, faster decay of the excitation, and band dispersion. However, the absence of a significant dependence of the peak positions on the angle of incidence, along with the small broadening of the vibronic structure, indicates little dispersion of these excitons (i.e., that the excitation is fairly well localized). As expected from the strength of the exchange interaction and the presence of electron resonances in the low-energy range, singlet-triplet transitions are prominent in the spectrum of Figure 12. This is a general feature of slow electrons which tend to produce HREEL spectra having much more intensity for low energy electronic transitions as compared to those produced by fast ones.

This latter characteristic is well illustrated in Figure 13 which shows the electron-energy-loss spectra of butadiene and cyclopentadiene [193] condensed on 10 ML argon films recorded at $\theta_0 = 14°$ and at a constant primary energy of 9.5 eV. The scattered electrons are detected at $\theta_r = 45°$. The thickness of the butadiene films corresponds to a monolayer coverage, whereas cyclopentadiene films are at least twice as thick. The symmetry of each electronically excited state is indicated Figure 13. Notice the decrease in the inelastically scattered intensity above 6 eV which continues up to the energy (9.5 eV) of the primary beam (not shown). For solid butadiene [186] and butadiene in 3-methylpentane [44], electronic excitation with fast electrons or photons begins around 5.5 eV (i.e., at the energy of the ^1B_u state). No signal has been reported for solid cyclopentadiene in the 2-6 eV energy loss range with these latter excitation sources. In hexane solution, the first transition to an excited state is observed in the spectral range 4.5-6 eV [92].

VIb. Luminescence and metastable production

In the last examples, the electronically excited states are fairly well localized at particular sites within the disordered molecular solid. The following examples on luminescence, desorption of metastable atoms from pure RG films, as well as desorption of metastable atoms and molecules from doped RG substrates, illustrate excitonic motion. They also indicate that excitons can be vehicles for transporting the energy of secondary electrons to the surface of a specimen irradiated by high-energy particles.

Figure 14 exhibits the temporal sequence of desorption patterns recorded from 100 ML Ar(111) films [81] with the apparatus shown in Figure 4. The incident electron energy was 14.5 eV; thus, only 2.5 eV above the threshold for excitation of bulk excitons. The electron beam was striking the target at 18° from the normal

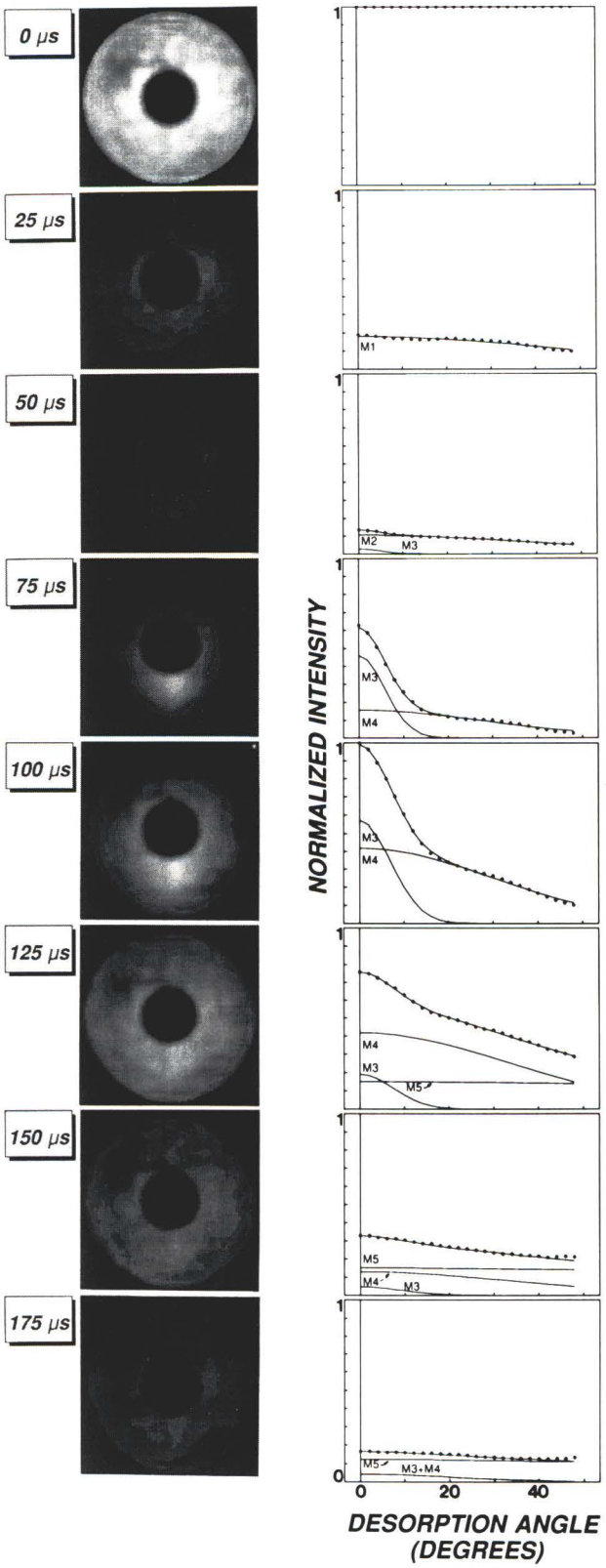

Figure 14 (at right). Time-resolved Ar^* desorption patterns from an Ar(111) film stimulated by 14.5-eV electrons. The electron pulse is on for 5 μs and the detection windows are 25 μs wide. The indicated time corresponds to the difference between the leading edges of the two pulses; the average time of flight for each pattern is 10 μs higher. On the right-hand side of each pattern, the normalized azimuthally integrated intensity distribution (dots) is given as a function of the polar angle, together with the contributions of the different desorption components.

---

for 5 μs every 300 μs, and the data collection was restricted to a time window 25 μs wide. The delay between the electron pulse and the acquisition window was increased in steps of 25 μs. The first pattern (labeled 0 μs) is attributed to photons emitted during the decay of excited states either within the bulk of the film or at the surface, or after ejection into the vacuum. The signal in the subsequent time windows (labeled 25 to 175 μs) is due to metastable particles, since all the known fluorescent states have lifetimes much shorter than the width of the detection time window [206]. The intensity and the angular distribution of the desorbed metastable particles change with flight time. The intensity has decreased considerably at 25 μs in comparison with the photon signal, but it is still very broad. At 75 μs, a distinct feature appears indicating a narrow desorption cone. At 100 μs, the signal has increased its intensity across the entire detector and is now very bright in the region of the narrow cone. This cone is centered on the surface normal and has a FWHM of 8°. The signal indicates a fine beam of metastable atoms ejected normally from the surface with a KE of roughly 50 meV. The narrowness of this distribution is quite surprising considering the small KE of the ejected atoms, which makes them sensitive to surface imperfections and phonon scattering. At 125 μs, a bright diffuse signal dominates over the narrow distribution. As the time delay increases, the signal becomes more diffuse and the intensity decreases.

On the right-hand side of each pattern in Figure 14, the normalized azimuthally integrated intensity distribution (dots) is given as a function of the polar angle θ together with the contributions of metastable desorption components of different KE and angular distributions (M1-M5) which are extracted from mathematical analysis of these patterns [81]. The presence of different components appears in Figure 15 where the TOF spectra of metastable Ar for desorption angles with respect to the surface normal between 0° and 50° are displayed. Changes in the TOF spectra desorption angle are due to several individual components with different angular distributions which are superimposed in the total desorption

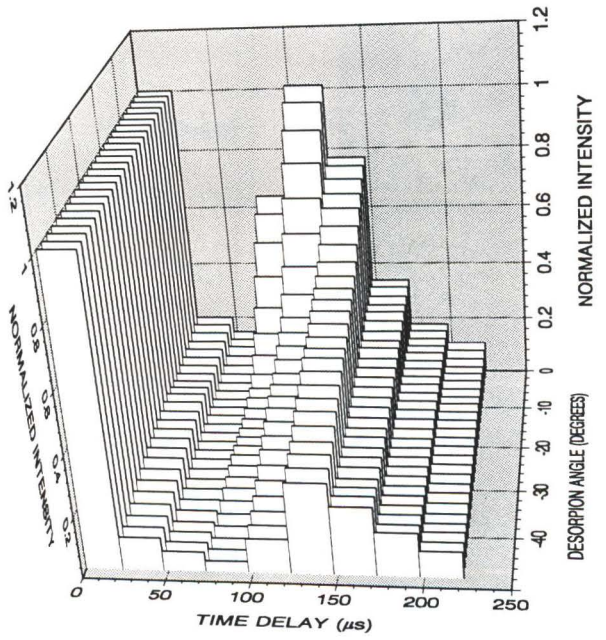

Figure 15. Metastable Ar signal as function of time and desorption angle. For each angle, the signal is normalized to the photon signal (first time-window, 0 to 25 μs).

---

yield. More information on the different velocity components has been obtained from high-resolution TOF spectra [81] in which the five distribution M1-M5 presented in Figure 14 can be discerned. These components have KE distributions with maxima located at 19, 36, 53, 85, and 345 meV ($\pm$ 10%), with the two lowest energy signals being more intense. The three lowest energy components were attributed [81] to metastable Ar emission in vacuum due to a "cavity" expulsion mechanism [27] resulting from forces exerted on the excited state of Ar which occupies more space in the lattice than ground state Ar. These forces are repulsive due to the negative electron affinity of bulk Ar, and thus, the excited atom is ejected into the vacuum when near the surface.

The 53-meV KE component (M3) has the narrow angular distribution of 8° FWHM with respect to the surface normal, while the others are broad. The sharpness of the angular distribution of the 53 meV component has been interpreted [81] to be the result of nuclear zero point motion in the undistorted crystalline environment. The 19- and 36-meV components are, according to recent molecular dynamics studies [28], the result of emission from different defect sites at the surface, where the net component of the forces acting on Ar^* lies off the specular direction. This condition necessarily broadens the desorption pattern. The 85- and 345-meV components result from the dissociation of excited dimer states described in Figure 16, which also provides a schematic survey of processes leading to photon and metastable emission in Ar(111).

Comparison with luminescence studies of condensed Ar indicates that the observed photon signal contains contributions from the radiative decay of several types of excited species as shown in Figure 16; i.e., free-exciton (FE) states, trapped-exciton states, and excited atoms and dimers ejected into the vacuum [28]. The high probability of self-trapping is revealed by the fact that the luminescence spectrum [76] is dominated by the decay of atomic (a-STE) and molecular (m-STE) self-trapped excitons, which are thought to resemble an excited Ar atom and an Ar excimer, respectively, embedded in the lattice. The a-STE arises from the relaxation of a bulk or surface FE. Self-trapping is possible as an atomic surface state or as a molecular Ar state within the bulk, but ejection of free excited Ar dimers has been observed in vacuo [145, 146]. Emission from these species has been identified as band W for the unrelaxed, and M for the relaxed, Ar states, respectively [76]. Band M in the solid (i.e., the m-STE) emits UV radiation at 9.72 eV. The relatively long lifetime (1.2 μs) of the m-STE [206] suggests that it is essentially this state which is responsible for the photon signal in Figure 14. In fact, the high-resolution time dependence of the photon signal can be described approximately by assuming decay from the m-STE state exclusively, indicating that the contribution of transitions from the free-atom and a-STE states is small. The delay times attributed to metastable particles ($t > 25$ μs) are much larger than any fluorescence lifetime previously seen in luminescence from Ar films [206]. It is therefore possible that both of the lowest metastable Ar states $\{(3p^5 4s)\ ^3P_2$ and $^3P_0\}$ contribute to the metastable signal. Their lifetimes are 55.9 and 44.9 seconds, respectively.

In addition to time-resolved patterns at a fixed electron energy, the apparatus described in Figure 4 can measure the incident-electron-energy dependence of the UV-photon and metastable signals [80, 84]. As an example, such functions are shown in Figure 17 for the UV-photon signal arising from condensed films of pure Kr and Xe having a thickness of about 25 ML. The photon signal is interpreted as emission from free-exciton states and relaxed m-STE states (M band). The W band, the a band (see Figure 16), and the free-atom emission lines are very weak or absent in Kr and Xe. In a simple picture, this behavior can be attributed to the negative energy of the band gap, meaning no cavities and no cavity expulsion of excited atoms or dimers. It is consistent with the very weak metastable-desorption signal observed [84] for pure Kr and none for pure Xe over the range of electron energies 5 to 25 eV. For both rare-gas films, the photon signal shows a strong

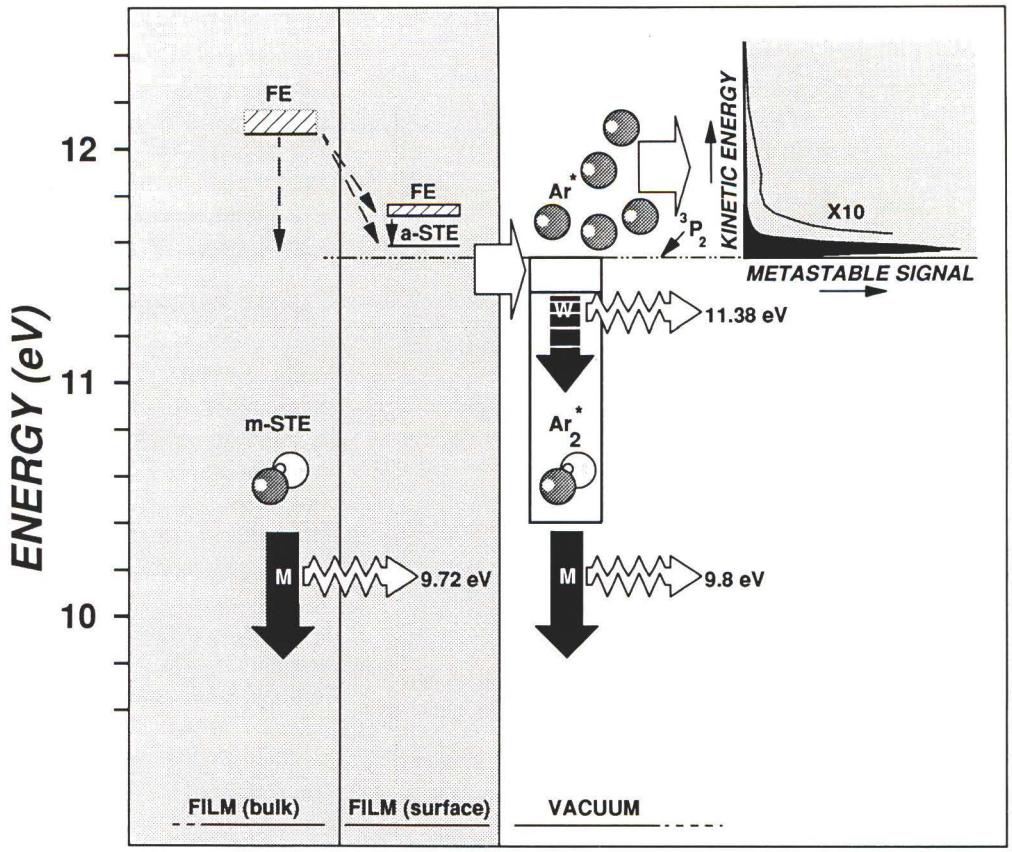

Figure 16. Schematic survey of the various excited states of Ar in the bulk of a film, at its surface, and in the gas phase. The abbreviations and references are mentioned in the text. The observed dependence of the signal on the kinetic energy of the metastable particle is sketched in the inset.

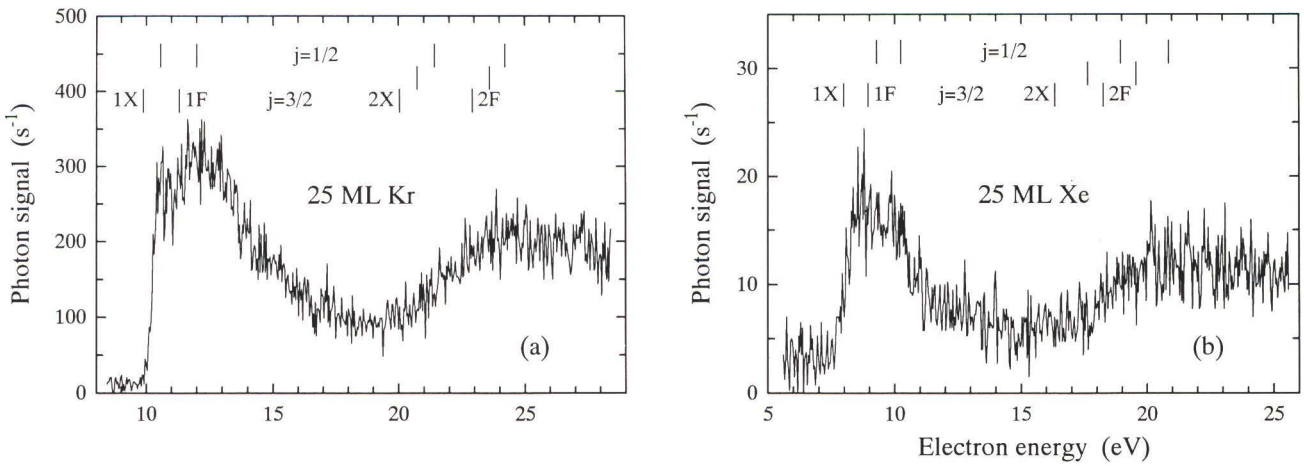

Figure 17. UV-photon signal from (a) a 25 ML Kr film and (b) a 25 ML Xe film on Pt(111) as function of incident-electron energy. The lines indicate the values of $mE(n = 1, b) + V_o$ and $mE_{Gap} + V_o$, m = 1, 2 for the j = 3/2 and 1/2 systems (X denotes the n = 1 bulk exciton and F the free-electron-hole pair).

---

dependence on the electron energy with two regions of pronounced photon yield being discernible. The two broad peaks in each excitation function of the total luminescence signal are related to the interplay between creation of excitons and free-electron-hole pairs [84].

Metastable-particle desorption has also been detected for Xe-, N_2- and CO-covered multilayer Kr films [84, Shi *et al.*, unpublished observations] as well as N_2 and CO covered multilayer Xe films [86]. In all cases, electronic energy transfer from the bulk of the RG to surface atoms or molecules was deduced from experimental observations. Figure 18 shows the metastable yield from a 50-ML Xe film covered with a single ML of N_2 and CO molecules. The metastable signal is due to N_2 and CO molecules, respectively, desorbed in metastable electronic states by 7-26 eV electrons [86]. The inter-

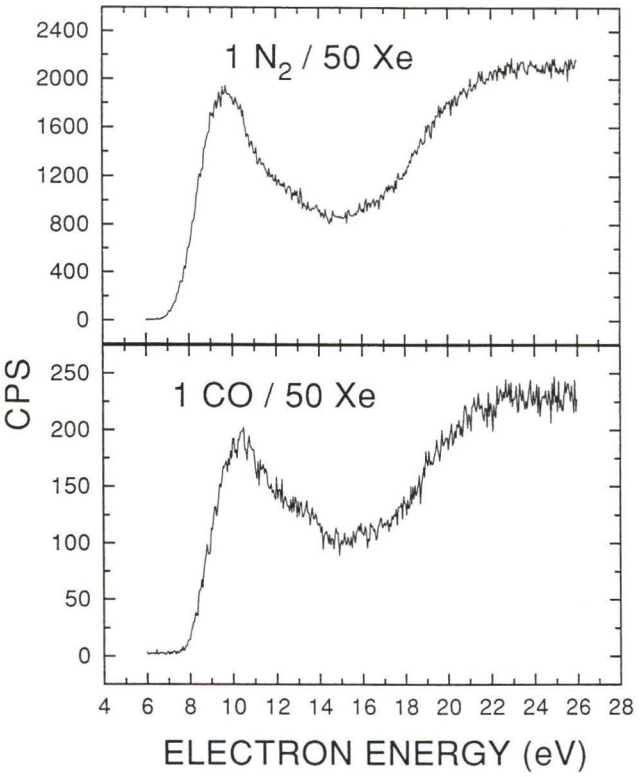

Figure 18. Yield function of metastable-particle desorption from a 50 monolayer (50 ML) Xe(111) film covered by a monolayer of N_2 and by a monolayer of CO.

---

pretation of the MP signal as due to N_2^* is based on the elimination of other possible candidates, Xe^* and N^*. Xe^* atoms do not desorb from a pure Xe film under the present experimental conditions and N^* species formation would involve the dissociation of a N_2^* state having an energy higher than 16 eV since the lowest dissociation limit is close to 10 eV and the internal energy of the metastable fragment must be at least 6 eV to trigger the detector. A similar reasoning applies to CO. As shown in Figure 18, the actual energy threshold for the metastable particle desorption for N_2 and CO lies around 7 and 8 eV, respectively. For these molecules there are a number of metastable states [50] that are sufficiently low in energy to match the threshold of the excitation function and possess sufficient internal energy to trigger a signal at the detector (e.g., $A^3\Sigma_u+$, $B^3\Pi_g$, $W^3\Delta_u$, $a^1\Pi_g$, for N_2).

The shape of the yield functions for N_2^* and CO^* resembles very much that for UV luminescence from the pure Xe(111) film, which is shown in Figure 17. The MP and UV-photon yields have very similar energy thresholds and peak features. However, the MP signal observed at the detector is an order of magnitude smaller for CO. Based on these comparisons and time-of-flight data for N_2^* and CO^*, it has been suggested [86] that most of the MP signal arises from excitons created by electron impact within the bulk of the Xe film, which reach the RG film surface and then transfer their energies to surface N_2 or CO molecules. The metastable N_2 and CO species thus created can desorb if, according to momentum and energy conservation rules, sufficient KE can be imparted to the molecule by the exciton which moves to the surface with momentum dictated by the lattice parameters of the Xe(111) film. This energy transfer is accompanied by vibrational excitation in the electronic excited state of N_2 and CO which weakens the surface-molecule bond and promotes desorption. This mechanism is particularly efficient if the excited adsorbates cannot surpass the surface energy barrier in the first step, and sufficient time is available for surface bond rupture through energy transfer from the internal vibrational excitation of the molecule to the adsorbate-surface bond. When the adsorbed molecule is in a vibrational energy level which is degenerate with some continuum state of the surface-molecule bond, cross-over into the latter state will lead to desorption of the molecule in a lower vibrational level. The feasibility of this mechanism has been demonstrated experimentally and theoretically [31, 64]. In the present case, the molecules on the surface are initially excited to high vibrational levels of the metastable electronic states. Assuming that the radiative decay on the surface of the films is similar to the gas-phase processes, the lifetime of the N_2 $B^3\Pi_g$ and CO (a' and d states) [82] is more than 6 orders of magnitude larger than the periods of molecule-surface modes. It is therefore sufficiently long to allow desorption via transfer of vibrational energy to molecule-surface modes [64].

VII. Molecular Dissociation

Above a certain energy threshold, electrons impinging on isolated or condensed molecules can cause disruption of internuclear bonds which leads to fragmentation. Depending on the intermediate state involved and charge exchange processes, the fragments can be either neutral, or positively or negatively charged. For molecular solids or molecules condensed on dielectric films, dissociation caused by the impact of 0-30 eV electrons can arise via the DEA process described in section **II**, by dissociation of an excited state produced either via resonance (see Figure 1) or direct scattering and dipolar by dissociation (DD, i.e., for a molecule AB: $e + AB \rightarrow AB^* + e \rightarrow A^- + B^+ + e$).

VIIa. Dipolar dissociation (DD)

The DD process has been observed in both negative [150, 151, 157, 158] and positive ion [70, 71, 115, 147,

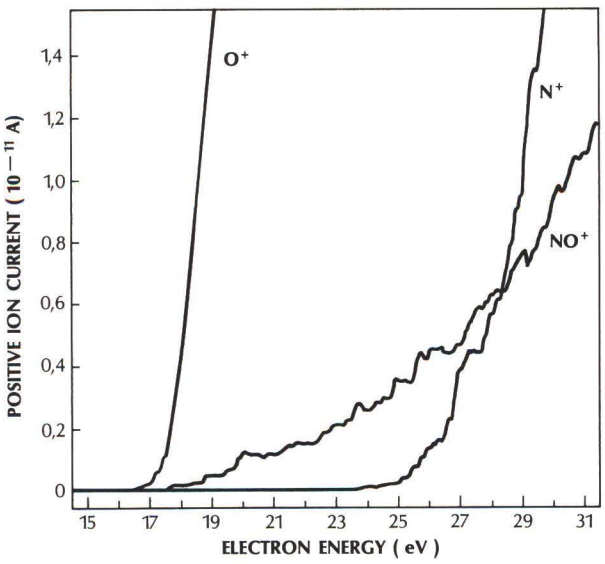

Figure 19. Electron stimulated desorption (ESD) yields of O^+, N^+ and NO^+ ions produced by electron impact on a multilayer film composed of 20% volume O_2 and 80% volume N_2.

188, 189] yields desorbed by electron impact from molecular solid films. The ESD yields of O^+ and N^+, from a multilayer film of 20% volume O_2 and 80% volume N_2, shown in Figure 19 arise from DD of N_2 and O_2 in the multilayer film [Sanche and Parenteau, unpublished]. The data indicate the threshold energy for observation of the process by ESD (i.e., ~ 17 eV for $O_2^* \rightarrow O^+ + O^-$, and ~ 25 eV for $N_2^* \rightarrow N^+ + N^-$, where the N^- autoionizes almost immediately). Within this low-energy range, DD is the only process capable of expelling positive ions in vacuum; excited ionized states usually lie beyond this energy range and ionization producing a ground state cation ($e + AB \rightarrow AB^+ + 2e$) cannot produce this latter with sufficient KE to overcome its polarization potential. As we shall see in the next subsection, a rise in anion ESD yields is also observed near the energy threshold for DD; but, it is not as sharply defined as in the cation yield function because the usual presence of transient anions dissociating into a neutral and an anion fragment often mask the DD threshold.

VIIb. Dissociative electron attachment (DEA)

The DEA process constitutes a particular channel for the decay of molecular transient anions (Figure 1) formed within molecular solids and near their surfaces. ESD of anions by DEA arises from transient states which dissociate before autoionization. Since a given molecular configuration of a transient anion appears at a well-defined energy, each peak in the electron-energy dependence of the anion ESD yield at low energies

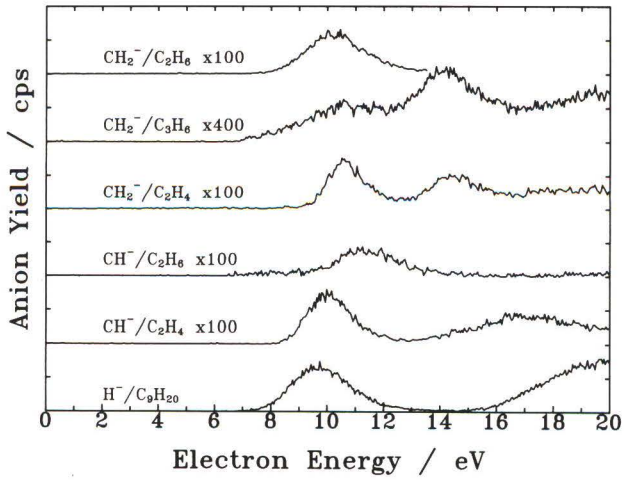

Figure 20. Energy dependence of the H^-, CH^- and CH_2^- ESD yields produced from multilayer films of C_9H_{20}, C_2H_6, C_3H_6 and C_2H_4 condensed on a Pt substrate. Each division of the vertical scale corresponds to 5,000 counts per second (cps). The gain factor is indicated for each CH_2^- or CH^- yield function.

---

identifies the energy of a particular resonant state. Such dissociating states have now been observed by electron trapping [17, 159, 165] and ESD [7, 8, 9, 10, 11, 12, 17, 60, 61, 62, 94, 95, 118, 121, 122, 148, 149, 150, 151, 152, 153, 156, 157, 158, 159, 161, 162, 163, 164, 165, 173, 180, 181, 185] techniques near the surfaces of a variety of molecular solids.

Anion ESD by DEA is exemplified in Figure 20 by the energy dependence of H^- yields desorbing from multilayers of n-nonane condensed on Pt and the CH_2^- and CH^- yields from C_2H_6, C_2H_4 and C_3H_6 multilayer films on Pt [151]. Each peak in these yield functions locates the energy of a transient anion (i.e., $C_9H_{20}^-$, $C_2H_6^-$, or $C_2H_4^-$), which dissociates into a stable anion and a neutral fragment. The rise near 16 eV in the bottom curve is due to DD (i.e., $e + C_9H_{20} \rightarrow C_9H_{19}^+ + H^- + e$). Notice that this process is practically absent in the other data. In all hydrocarbons studied so far [150, 151, 152] (i.e., C_nH_{2n}, n = 2,3,4, C_nH_{2n+2}, n = 1,2,4 to 9), only a single peak is present in all H^- ESD yield curves; its magnitude is comparable to that at 20 eV arising from DD.

Besides the work on these saturated and unsaturated hydrocarbons, DEA features have been observed in the O^-, C^-, Cl^-, F^-, Br^-, D^- and H^- ESD yield functions measured from molecular solids formed by condensing O_2, NO, CO, Cl_2, N_2O, CH_4, CF_2Cl_2, CCl_4, $CDCl_3$, CD_2Cl_3 CH_3Cl, CH_3Br, CH_3OH, CD_3OH, CH_3OD, CF_3I, $CFCl_3$, CF_4, D_2O and H_2O molecules on a metal substrate [7, 8, 9, 10, 12, 62, 94, 95, 118, 121, 122, 149, 153, 156, 161, 163, 172, 185]. Furthermore, the

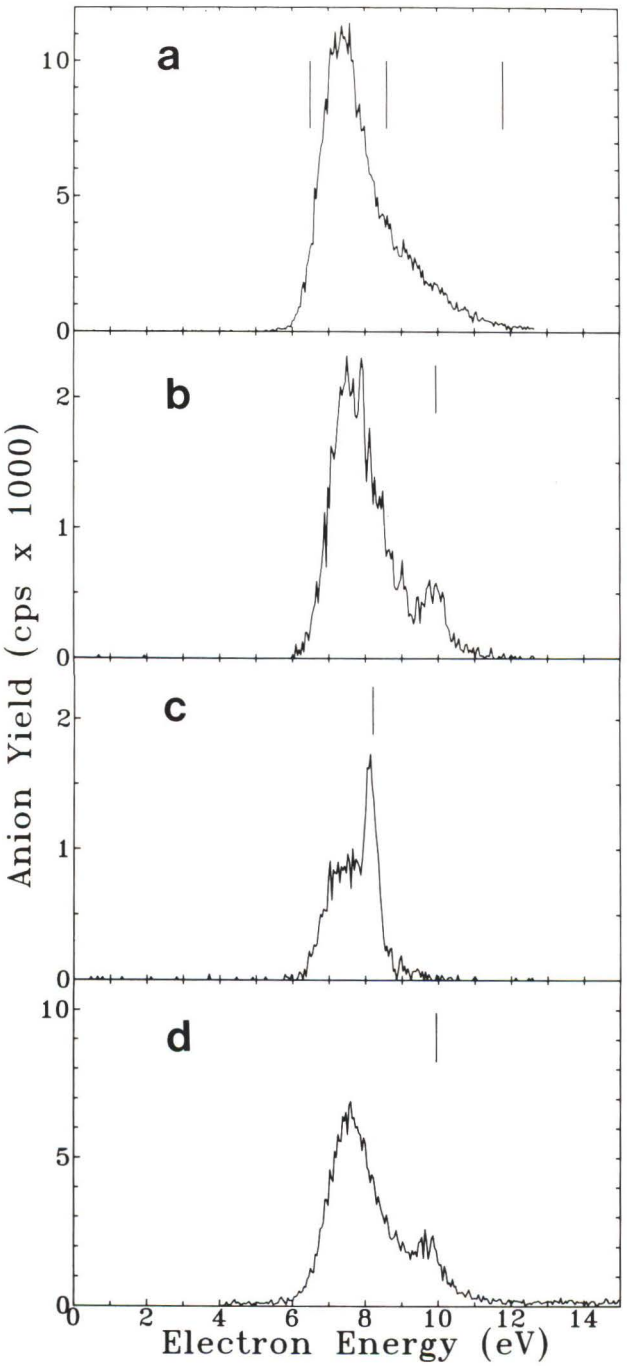

Figure 21. D^- yield functions produced by electron impact on: (a) 6 monolayer (ML) of D_2O condensed on Pt; (b) ~0.1 ML D_2O adsorbed on 24 ML Kr; (c) ~0.1 ML D_2O adsorbed on 50 ML Xe; (d) ~0.1 ML H_2O adsorbed on 40 ML Kr. (a), (b) and (c) were measured with an incident angle of 50 degrees, while (d) was measured with an incident angle of 70 degrees. The vertical bars in (a) are positioned at the energy of the gas-phase DEA resonances. Those in (b), (c) and (d) show the lowest exciton energies for each rare gas substrate.

anion-complexes $Ar{\cdot}O^-$, $Ar{\cdot}Cl^-$ were produced by ESD from Ar matrices containing N_2O and Cl_2, respectively [175], and O^-, $Ar{\cdot}O^-$, $Kr{\cdot}O^-$, O_3^- (or $O_2{\cdot}O^-$) and O_2^- were observed by ESD from solid rare-gas matrices containing O_2 [175, 180]. In CO and N_2 matrices, the electron energy dependence of the O^- yields from O_2 was reported by Azria *et al.* [10]. The ESD yield functions from submonolayer O_2 adsorption onto C_2H_4 C_2H_6, N_2O, CH_3Cl and H_2O multilayer films [60, 61] and solid RG [157, 158, 181] surfaces have also been measured. Solid rare-gas surfaces served as molecular solid substrates for other anion ESD experiments with submonolayer coverages of the molecule H_2O, D_2O, CF_4, $CFCl_3$, methanol, benzene and various halomethanes and aliphatic hydrocarbons [94, 121, 122, 148, 152, 153]. In these systems, the RG electronic excitations (i.e., the excitons) were found to influence the anion ESD yields, arising from dissociating transient anion states [152]. This is explained in the next paragraph by taking rare gas solids partially covered by D_2O as example.

Figure 21a shows the DEA yield function of D^- produced by ESD from a 6 ML film of D_2O condensed on Pt [148]. This function is dominated by a single peak at an incident energy of 7.4 eV, with a FWHM of 1.5 eV. This peak and its profile are strongly reminiscent of the DEA anion yields with 6-8 eV electron impact in H_2O vapor [96] and $(D_2O)_n$ clusters [77]; it has been interpreted to arise from the dissociative decay of the $^2B_1$ $(D_2O)^-$ state, with possible contributions from the $^2A_1$ state. The D^- yield function in Figure 21b was produced by electron impact on ~ 0.1 ML of D_2O physisorbed on a 24 ML Kr film [148]. For $E_i < 9$ eV, the shape of the dominant $^2B_1$ resonant peak is similar to that of the pure D_2O results, but for E_i = 9.5-10.8 eV a narrow peak appears in the yield function. This peak is the only significant departure from the line shape of Figure 21a. A similar behavior is observed when ~ 0.1 ML D_2O is condensed on a thick Xe film substrate, as shown in Figure 21c. A sharp peak is now observed for E_i = 8.0-8.5 eV with a FWHM of 0.3 eV, which is probably limited by the energy resolution of the electron source. As the coverage of the RG substrate by D_2O is increased, the contribution of the sharp peak to the overall magnitude of the signal is reduced, such that the DEA D^- yield from 2 ML D_2O on 50 ML Xe or Kr is identical to that from multilayer D_2O adsorbed directly onto the Pt foil. The position of the narrow peak for 0.1 ML D_2O on Kr is the same for an incident angle of 50° (Figure 21b) and 70° (Figure 21d). This measurement excludes the possibility of diffraction effects. The narrow peak is found at E_i = 9.8 eV on the Kr substrate and at E_i = 8.1 eV on the Xe substrate (i.e., 0.1-0.4 eV below the lowest exciton energies for each substrate). Measurements of the DEA anion yields from submono-

layer C_2H_6 targets on the previously mentioned substrates have produced similar results [152]. Such enhancement of anion yields near the energy of the lowest electronic excitation of the substrate has been interpreted [152] to result from the formation of RG core-excited resonances at the substrate surface followed by **transfer of the excitation energy and charge to the adsorbate molecule**, causing the latter to form a transient core excited anion which dissociates.

The energy distribution of the ions produced by DEA has been reported for Cl^-, O^- and H^- from condensed Cl_2, O_2 and H_2O, respectively [7, 8, 12, 62, 149], as well as for O^- and H^- ESD from condensed CO [9] and CH_3OH [122], respectively. This analysis has been found to be particularly helpful to study the perturbation imposed by neighboring targets on the gas-phase DEA mechanism. These perturbations can be classified into two major categories: (1) those that arise from a fundamental modification of the properties of the intermediate anion state and its dissociation process, and (2) those that arise from multiple electron scattering prior to electron attachment or from scattering of the anion produced by DEA. This latter process is usually referred to as post dissociation interaction (PDI). We discuss these perturbations with pertinent examples in the rest of this section.

VIIc. Multiple electron scattering and post-dissociation interaction (PDI)

Electrons striking a target, composed of molecules condensed on a substrate, can scatter multiply before attaching at a particular molecular site to form a temporary anion. Thus, multiple energy losses to phonons and intra-molecular vibrations can broaden DEA peaks in the yield functions; these latter can even exhibit new peaks if electronic excitation prior to anion formation is sufficiently intense. The dissociation dynamics of condensed Cl_2^-, reported in this section are illustrative of the effects of electron energy losses before attachment.

The dependence of the Cl^- signal on the energy of electrons impinging on approximately one and four ML thick films of Cl_2 condensed on Pt is shown at the bottom and the top of Figure 22, respectively [7]. The inset shows the energy dependence of the Cl^- yield in the low-energy region obtained on a monolayer film with the electron lens adjusted to transmit low-energy (1-3 eV) electrons with high efficiency. We see from these curves that at low coverage the Cl^- yield exhibits two structures, one appearing as a shoulder around 2 eV and one as a peak around 5 eV. At higher Cl_2 coverage, another peak appears at 11.5 eV in the ion yield. Except for this later peak which cannot be assigned to a simple scattering process, there exists a relatively good agreement between the peak positions in Cl^- yields from

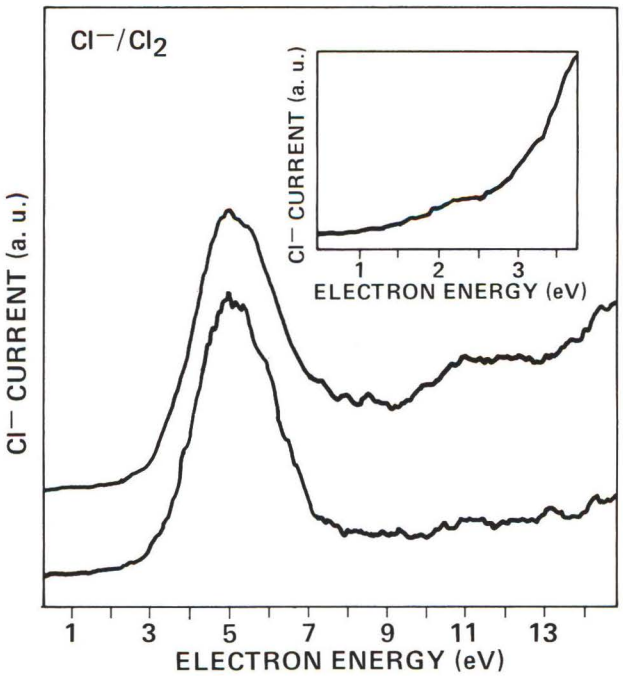

Figure 22. The lower curve represents the energy dependence of the Cl^- yield produced by electron impact on a one-layer-thick film of condensed Cl_2. The upper curve was recorded with a four-layer-thick film. The curve in the inset was recorded on a single-layer film with the electron lens adjusted to transmit principally low-energy (1-3 eV) electrons.

---

condensed and gaseous Cl_2 in the 1-8 eV energy range. From this agreement, the 2 eV and the 5 eV peaks in condensed Cl_2 have been ascribed, respectively, to DEA processes involving the $^2\Pi_g$ and $^2\Pi_u$ Cl_2^{-*} core-excited resonances.

Figure 23 shows ion-energy distributions in the incident electron energy range of the $^2\Pi_u$ Cl_2^{-*} resonance [7]. These distributions exhibit structures shifting with incident energy and they are much broader than the ion energy resolution of the apparatus. Their behavior can be explained by considering the dynamics of DEA reactions on a diatomic molecule in free space. In this case, the excess energy is shared between the dissociating fragments as KE according to momentum and energy conservation laws (i.e., in proportion to a parameter β which is the ratio between the mass of the ion and the mass of the molecule) [7]. In the case of free homonuclear diatomic molecule, β is 1/2; then, the curve representing the KE of the negative ions as a function of incident electron energy is a straight line with a slope 1/2. This is, in fact, what is observed for the high energy peak in the Cl^- ion KE distributions, the positions of which can be determined precisely from Figure 23. Therefore, the formation of these energetic Cl^- ions

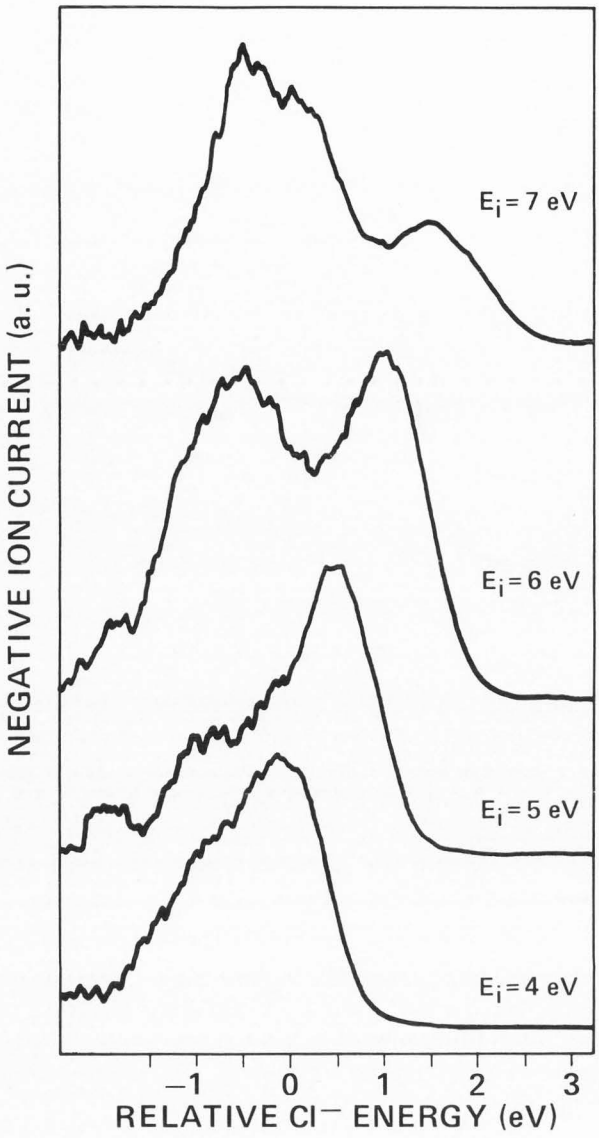

Figure 23. Kinetic energy (KE) distribution of Cl^- ions produced by electron of energies E_i = 4, 5, 6 and 7 eV incident on a monolayer Cl_2 film. The ion energy is referenced to the maxima in the KE distribution of Cl^- ions at E_i = 4 eV.

---

arise from a single scattering DEA process via the $^2\Pi_u$ Cl_2^{-*} resonance. This result indicates that no significant amount of momentum is transferred to the lattice as the Cl^- recedes from the surface.

The other peaks in Figure 23 have been associated [7] with multiple scattering of incident electrons; i.e., to electrons which have suffered vibrational and electronic losses before attaching to Cl_2 molecules to form the $^2\Pi_u$ or the $^2\Pi_g$ Cl_2^{-*} states which dissociate. From comparison with threshold excitation studies of gaseous Cl_2 by electron impact (i.e., from the position of the excited electronic states of Cl_2), it has been found that incoming electrons may first excite Cl_2 in the *B* or *C* electronic states and have enough residual energy to produce a DEA dissociation via the $^2\Pi_u$ or $^2\Pi_g$ Cl_2^{-*} resonances. In other terms, the reaction path

$$e(E_i) + Cl_2\,(^1\Sigma_g^+) \rightarrow Cl_2^{*}\,(B \text{ or } C) + e\,(E_i - E^*) \quad (R1)$$

followed by

$$e\,(E_i - E^*) + Cl_2\,(^1\Sigma_g^+) \rightarrow$$
$$Cl_2^{-*}\,(^2\Pi_u \text{ or } ^2\Pi_g) \rightarrow Cl^-\,(^1S) + Cl\,(^2P) \quad (R2)$$

is energetically possible. The relative positions of the structures observed in the KE distributions shown in Figure 23 are consistent with electronic excitation, assuming that, Cl^- ions carry off half of the excess DEA reaction energy. Furthermore, the KE distributions of Cl^- ions obtained in the energy range of the third peak around 11.5 eV in Figure 22 indicate that these ions have about the same KE as those of the 5 eV peak. Consequently, the 11.5 eV peak in the yield function was ascribed to Cl^- ions formed via the $^2\Pi_u$ Cl_2^{-*} resonance by electrons which have suffered energy losses through the excitation of electronic Cl_2 states lying between about 3 and 8.5 eV [7].

PDI of stable anions formed by DEA can also considerably modify anion KE distributions such as those shown in Figure 23. For example, the KE distributions of O^- ions from ESD from condensed multilayer CO were interpreted by invoking the PDI reaction [9]

$$O^-(^2P) + CO\,(^1\Sigma_g^+) \rightarrow CO_2^-\,(^2\Pi_u) \rightarrow CO\,(^1\Sigma_g^+, v) + O^- \quad (R3)$$

where v denotes vibrational excitation. This vibrational energy transfer reduces O^- velocities and hence the number of anions which can escape the induced polarization field at the surface.

VIId. Dependence of DEA on environment

The effect of a metal surface on ESD yields induced by DEA is shown in Figure 24, where each curve exhibits the ESD O^- yields for 1-20 eV electrons incident on 6.6, 3.3, 2.0, 1.0, and 0.3 ML of O_2 physisorbed on Pt [176]. The strong peak around 7 eV arises from the dissociation of unresolved $^2\Pi_u$ and $^2\Sigma_g^+$ quasi-bound O_2^- ions into the $O^-(^2P)$ + $O(^3P)$ limit [155, 180]. The less intense peak at 13 eV is caused by the creation of one or two $^2\Sigma^+$ states decaying essentially into the limit $O^-(^2P)$ + $O(^1D)$. As the film thickness diminishes, the transitory O_2^- ions are formed closer to the Pt surface, which increases the effect of the image charge on the molecular anion. The image charge modifies the lifetime of O_2^-

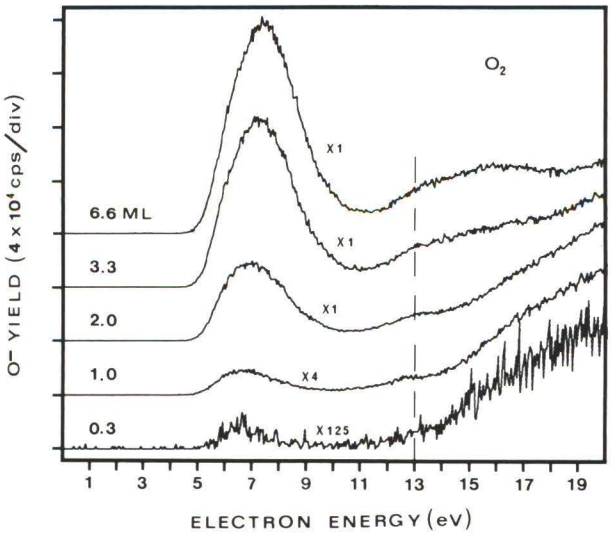

Figure 24. Energy dependence of ESD O^- yields for different O_2 coverage of a Pt substrate corresponding to 0.3, 1.0, 2.0, 3.3, and 6.6 ML.

---

which in turn affects the O^- yields [157]. The average KE of escaping O^- ions decreases with increasing induced polarization in the metal as the film thickness diminishes, thus also decreasing the ESD signal. The image charge can change the branching ratio between the trapped and desorbed anion states (i.e., between the $O^-/S + O$ and $O/S + O^-$ dissociation limit where S indicates the species remaining on the surface) because of the increase binding of the O^- ion to the surface in the presence of the metal substrate [157]. Finally, we must also consider that any change in the average O_2 orientation with film thickness would modify the O^- intensities by reorienting the outgoing O^- velocities as well as influencing the resonance parameters (e.g., the electron capture cross-section). For submonolayer coverage, surface quenching of the intermediate O_2^- state is probably the most efficient mechanism affecting the lifetime by causing neutralization of O_2^- (i.e., by electron transfer to the metal) before dissociation into $O^- + O$ fragments. At submonolayer coverage, the O^- signal survives, but it is two orders of magnitude smaller than that measured from multilayer films.

Metals are not the only materials which can alter the DEA process. Taking again as a reference DEA in pure O_2, the O^- ESD yields from O_2 under different environmental conditions [61] are shown in Figure 25. The yield functions in this Figure were produced by monoenergetic electrons impinging on 0.15 ML of O_2 condensed on different substrates. These latter were prepared by condensing 4 ML of (b) Kr, (c) C_2H_6, (d) C_2H_4, (e) N_2O, and (f) H_2O on a clean Pt surface held at a temperature of 20K. Curves (b) to (f) were recorded by

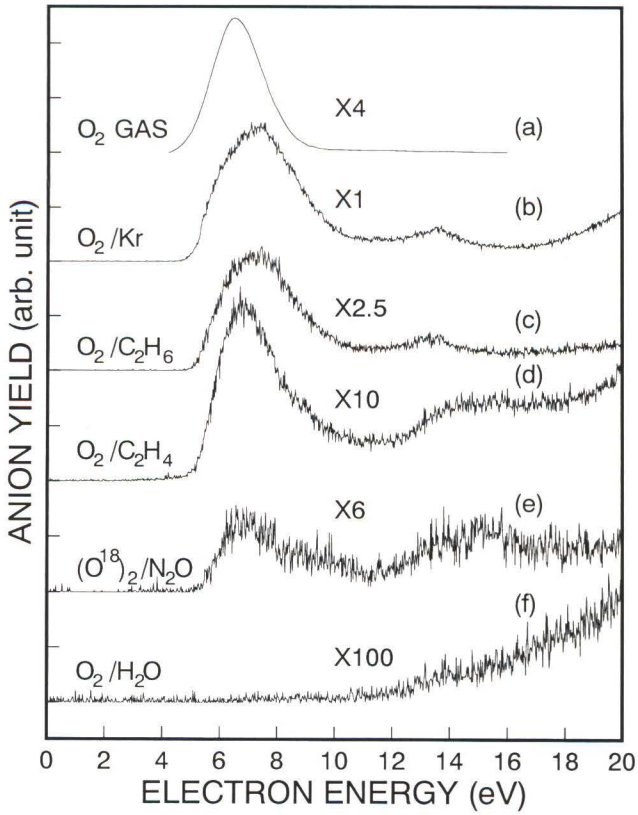

Figure 25. O^- yields produced by electron bombardment of (a) gaseous O_2 molecules, and (b) to (f) 0.15 monolayers of O_2 molecules condensed on 4 ML of Kr, C_2H_6, C_2H_4, N_2O and H_2O substrates, respectively. The number over each curve indicates the gain or amplification factor relative to curve (b). The relative magnitude of the O^- intensity in curves (b) to (f) is highly sensitive to the nature of the substrate; it is reliable within 5%.

---

keeping all experimental parameters the same, so that the relative magnitude of each curve is reliable within a 5% error. The 6.7 eV peak in Figure 25a is due exclusively to dissociation of the $^2\Pi_u$ state of O_2^- formed by gaseous electron attachment. Access to the Σ^+ states is symmetry forbidden in the gas-phase [155], whereas for condensed O_2 up to four $^2\Sigma^+$ states may contribute to the ESD anion yield below 16 eV [62].

Comparison of the O^- yields in Figure 25 clearly shows that dissociation of O_2 by DEA, is highly dependent on the environment of the O_2 molecule. For example from curves (b) and (d), one can estimate that dissociation via DEA is about an order of magnitude stronger when O_2 is surrounded by Kr atoms rather than by C_2H_4 molecules. Even between hydrocarbon substrates composed of molecules of similar molecular weight and size (i.e., C_2H_6 and C_2H_4), an almost threefold difference is seen in O^- yields. Within the limits of detectability, the

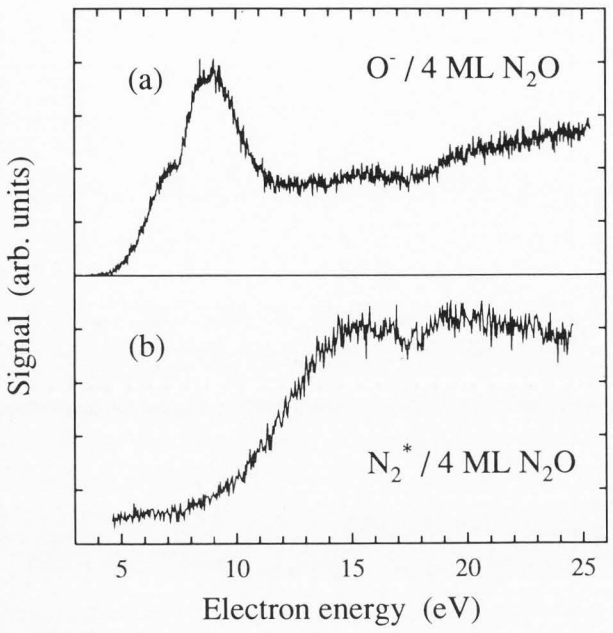

Figure 26. ESD yield function of **(a)** O^- and **(b)** metastable species from a 4 ML film of N_2O condensed on Pt.

DEA process is completely absent for O_2 condensed on amorphous ice (curve f)! As discussed by Huels *et al.* [61] different processes, including quenching, PDI and inelastic electron scattering, can account for such differences. The very small signal monotonically increasing from about 12 eV in (f) is largely due to DD ($e + O_2 \rightarrow O^+ + O^- + e$). From the noise level, the O^- signal from DEA is estimated to be at least three orders of magnitude smaller than that obtained with the Kr substrate. This translates into a cross-section of the order of 10^{-20} cm^2 for dissociating O_2 below 12 eV and lower than 10^{-19} cm^2 below 20 eV. These findings indicate that DEA, which is a major process leading to molecular dissociation by low-energy electron impact, can be controlled by modifying the molecular environment of the transient anion responsible for the damage.

VIIe. Dissociation from neutral states

Dissociation of a molecule near the surface of an atomic or molecular solid can also occur if the impinging electron excites directly a dissociative electronically excited state of a molecule. When one of the dissociating fragments is created in a metastable state, it is possible with the apparatus shown in Figure 4 to measure this process by detecting the metastable fragment. This is shown in the example of Figure 26b, where the curve represents the metastable desorption signal produced by 5 to 25 eV electrons impinging on a four-layer N_2O target deposited on Pt(111) [164]. The metastable signal is believed to be produced essentially by N_2^* metastable

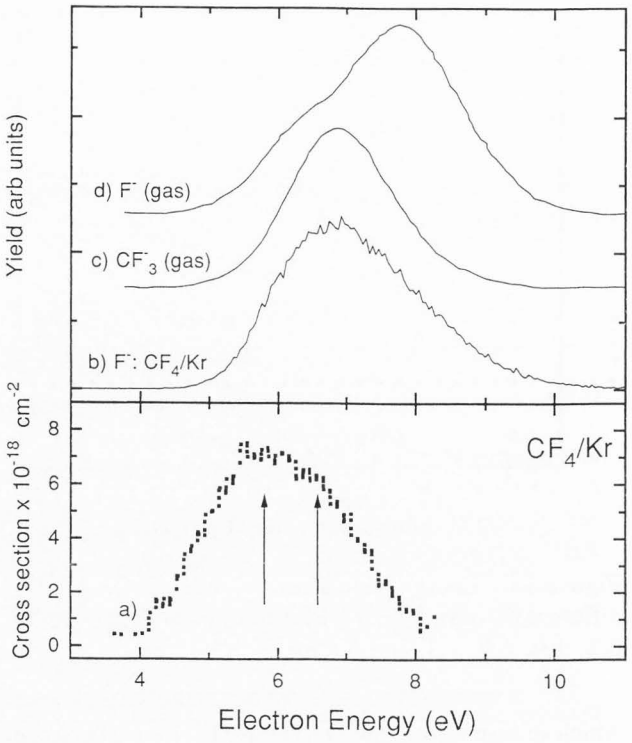

Figure 27. **(a)** Charge trapping cross-section for 0.2 ML CF_4 on 15 ML Kr. **(b)** F^- yield from 0.15 ML of CF_4 on 15 ML Kr. **(c)** and **(d)** Yield of CF_3^- and F^- respectively, from gas phase CF_4.

---

molecules arriving at the detector. The non-structured portion of the signal arises from direct excitation of one or many dissociative electronic states, i.e.,

$$e + N_2O \rightarrow N_2O^* + e \rightarrow N_2^* + O + e, \qquad \text{(R4)}$$

whereas, the broad peak near 15 eV which is superimposed on the rising background can be attributed to the reaction

$$e + N_2O \rightarrow (N_2O^-)^* \rightarrow N_2^* + O^-. \qquad \text{(R5)}$$

For comparison, the O^- ESD yield function from a 4 ML N_2O film is shown in Figure 26a. Here, the maxima at 7.0, 9.0 and 15.5 eV identify the positions of three dissociative N_2O^- states. Thus, the set of data in Figure 26b indicates that the maximum at 15 eV in the metastable signal is probably due to N_2^* arising from the decay of an $(N_2O^-)^*$ state into the dissociation limit $N_2^* + O^-(^2P)$. Accordingly, the 15.5 eV maximum in Figure 26a corresponds to reaction R5 and the other features result from the decay of two N_2O^- states into the ground state dissociation limit $N_2(^1\Sigma_g^+) + O^-(^2P)$.

VIII. Trapping of Low-Energy Electrons in Dielectrics

Secondary (i.e., low-energy) electrons are trapped within a dielectric and at its surface by specific processes. Within the low-energy range considered in this review article, free and quasi-free electrons can be thermalized by energy exchange with a group or cluster of atoms or molecules within the dielectric, by DEA, or by resonance stabilization (i.e., reaction 5 in Figure 1). The latter two processes have been shown to occur for O_2 on solid Kr [159, 165] and the former within H_2O clusters [17] also on a Kr surface. An example is given here of surface charging via DEA by submonolayer amount of CF_4 deposited on a Kr multilayer substrate [Bass *et al.*, unpublished].

Figure 27a shows how the charge trapping cross-section, measured by the method explained in section **IIIb**, varies as a function of incident electron energy for a small amount (0.15 ML) of CF_4 deposited on a 15 ML Kr film. The yield of CF_3^- and F^- ions from gas phase electron-molecule attachment [65] are shown in Figure 27, curves c and d, respectively. In the gas phase, the relative intensity of the two fragment ions [48] is $F^-:CF_3^- = 1:0.6$. Figure 27, curve b, represents the energy dependence of the yield of F^- desorbed from the film surface. It is apparent from Figure 27, that there exist similarities among these four curves and that the ESD and charge trapping phenomena, observed in the condensed phase, derive from essentially the same DEA process seen in the gas phase. However, close inspection of the gas phase data does reveal some difference. While CF_3^- formation is associated with a Gaussian-like profile around 6.8 eV, the F^- spectrum peaks at 7.6 eV and has a structure near 6.8 eV. This behavior has been interpreted as electron capture via two negative ion states, ground state CF_4^- and an electronically excited state [65, 117]. The anion ground state decomposes along repulsive energy surfaces via the complementary channels

$$CF_4^- (6.8\ eV) \rightarrow F + CF_3^- \qquad (R6a)$$

$$CF_4^- (6.8\ eV) \rightarrow F^- + CF_3, \qquad (R6b)$$

while the excited state yields exclusively F^-. Consequently, the F^- yield is composed of contributions from these two overlapping resonances. In addition to producing F^-, it is thought probable that CF_4^{*-} dissociates to form an excited CF_3^* radical that itself subsequently dissociates [65]:

$$CF_4^{*-} (7.6\ eV) \rightarrow F^- + F + CF_2. \qquad (R7)$$

In contrast to the ESD data, the charge trapping cross-section reveals two structures, indicated in Figure 27a by the two arrows: a maximum at 5.8 eV and a shoulder at 6.6 eV. This strongly suggests that at the surface of the film, both resonance mechanisms (R6) and (R7) are involved in the charging process. Indeed, a shift of 1 eV to lower energy of the gas-phase anions, to take into account the polarization energy at the Kr surface, places the two gas-phase resonances at the energy of the two structures seen in Figure 27a. The isolated-molecule cross-section for the production of individual anionic fragments [48] and for total DEA [63] have been measured and peak values found to be in the range (1.0-1.6) x 10^{-18} cm^2. The value obtained from the result in Figure 27, for the maximum charge trapping cross-section is 7.3 x 10^{-18} cm^2 $\pm$ 37% and is significantly larger than the gas phase cross-section by a factor of between four and seven. In fact, the enhancement in the condensed phase DEA cross-section is somewhat greater than this as some fraction of the F^- ions desorb from the film. Since no significant charging signal was observed below 4 eV and in the 8-11 eV range, it has been postulated that the main electron trapping mechanism below 11 eV is DEA. **This process not only efficiently dissociates CF_4, with a cross-section of about 10^{-17} cm^2, but it also creates a permanent charge (F^-) on the Kr surface.**

IX. Reactions Induced by Low-Energy Electrons

The radical atoms and anions produced with several eV of energy by dissociating neutral and transient anion states are expected to be highly reactive and lead to the formation of new products, when they react with neighboring atoms or molecules located within or at the surface of a solid. In fact, these species are so reactive that they are likely to form new products with almost any substance. The damage caused by low-energy electrons impinging on a molecular solid has been observed by measuring the total cross-section for disappearance of the initial constituents of the sample and by measuring specific degradation products during the time of bombardment. With the latter type of measurement, it has often been possible to specify the mechanism causing the damage by recording the incident electron energy dependence of the yields.

IXa. Total cross-section for specimen damage

With the type of experiment described in section **IIIf**, it has been possible to measure the total effective cross-section (σ_D) for degradation of n-hexane by 0-30 eV electrons [79]. The results obtained for a seven-layer n-hexane film are shown in Figure 28. Loss of the compound was found to begin at an incident energy (3.6 eV) well below the optical absorption threshold (7.4 eV) implying that either very low-lying triplet excited states

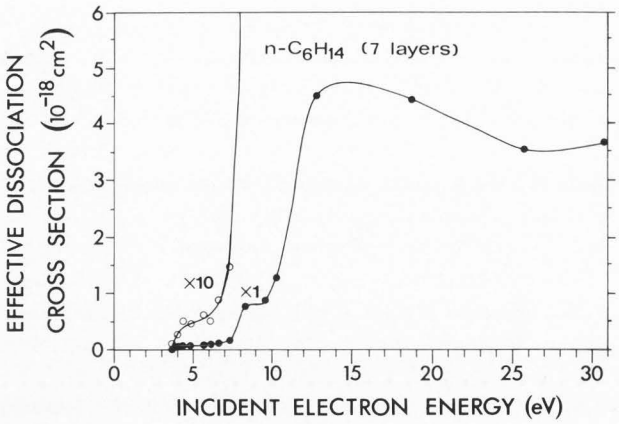

Figure 28. Measured values of the effective dissociation cross-section σ_D for a 7-ML n-hexane film in the incident energy range 0.5-31 eV.

---

are involved or that some evaporation of n-hexane occurs during the experiment. Electronic states of n-hexane are not expected below ~ 7 eV in the Franck-Condon region; it is therefore likely that the small signal below 7 eV arises from evaporation of the sample via vibrational heating by the high intensity electron beam. As mentioned in section **VI** for N_2 and CO condensed on Xe, coupling of intramolecular vibrational excitation to the molecule-surface bond can lead to desorption of excited surface molecules [86].

Near 7-eV, the sharp increase of σ_D can be related to the dissociative excitation of at least the first n-hexane singlet excited state which onsets at 7.4 eV. DEA of n-hexane is very similar to that for n-nonane shown in Figure 20. Hence, this process also contributes to σ_D in this energy range. Finally, above the ionization threshold, the energy dependence of σ_D does not follow the behavior expected from known gas-phase data [204, 205]. Neutralization of cations is probably quite efficient and not so often followed by decomposition. Dissociation in the range 8.5-31 eV is expected to arise essentially from superexcited states produced above 10 eV [79].

IXb. Specific mechanisms of damage

Measurements of H_2 production as a function of the energy of incident slow electrons on multilayer H_2O and hydrocarbon films have been applied successfully to specify the mechanisms leading to sample damage. Via mass spectrometry, Kimmel *et al.* [74] observed stimulated production of D_2 (H_2) during 5-50 eV electron-beam irradiation of D_2O (H_2O) amorphous ice. The upper limit for the D_2 (H_2) production threshold was found to lie at 6.3 ± 0.5 eV, well below the first excited state of condensed water at 7.3 eV. The D_2 (H_2) yield increases gradually until another threshold was reached at ~ 17 eV and continues to increase monotonically (within experimental error) up to 50 eV. The authors assigned the 6.3 eV threshold to the condensed phase (primarily surface) reaction

$$D^- (H^-) + D_2O (H_2O) \rightarrow D_2 (H_2) + OD^- (OH^-) \qquad \text{(R8)}$$

where the $D^-(H^-)$ is supplied by DEA (i.e., $e + H_2O \rightarrow H_2O^- \rightarrow H^- + OH$ as shown in Figure 21a). Above the threshold for electronic excitation (7.3 eV) the yield was also associated with the dissociation of Frenkel-type excitons below ~ 11 eV; above that latter it was attributed mainly to the recombination of D_2O^+ or D_3O^+, with quasifree or trapped electrons [74].

A number of ion-molecule reactions were also identified as contributors to sample damage at low electron energies from the observation of ion products resulting from the reaction of positive or negative ions with neighboring molecules near the surface of molecular solids. These ions were formed by dissociating neutral or anionic excited states first created by low-energy electron impact. The NO^+ signal in Figure 19 arises from such a reaction [Sanche and Parenteau, unpublished]. Figure 19 shows the result of an experiment where a 50 Å-film composed of 20% volume O_2 and 80% volume N_2 is bombarded with 15 to 31 eV electrons. The curve labelled O^+ was obtained by measuring the energy dependence of the O^+ signal. Similarly, the curves labelled N^+ and NO^+ represent the ESD yields of these cations, respectively. The O^+ signal can arise essentially from the reaction

$$e^- + O_2 \rightarrow O_2^* + e^- \rightarrow O^+ + O^- + e^-. \qquad \text{(R9)}$$

The onset of the reaction

$$e^- + N_2 \rightarrow (N_2^+)^* + 2e^- \rightarrow N^+ + N + 2e^- \qquad \text{(R10)}$$

lies around 25 eV. The magnitude of the O^+ signal is about four times higher than the N^+ signal and more than an order of magnitude larger than the NO^+ signal. Below 25 eV, since no N^+ ions can be formed, the NO^+ signal must therefore arise from the reaction of energetic O^+ with N_2. The possible reaction of N_2^+ with O_2 or O_2^+ with N_2 yielding $NO^+ + NO$ must be eliminated because any intermediate $N_2O_2^+$ state in the 17-25 eV range could not lead to NO^+ ions having sufficient KE to overcome the polarization barrier of the film. Furthermore, the coincidence of the energy threshold of the O^+ and NO^+ signals dictates interpretation involving the reaction

$$N_2 + O^+ \rightarrow N_2O^+ \rightarrow N + NO^+. \qquad \text{(R11)}$$

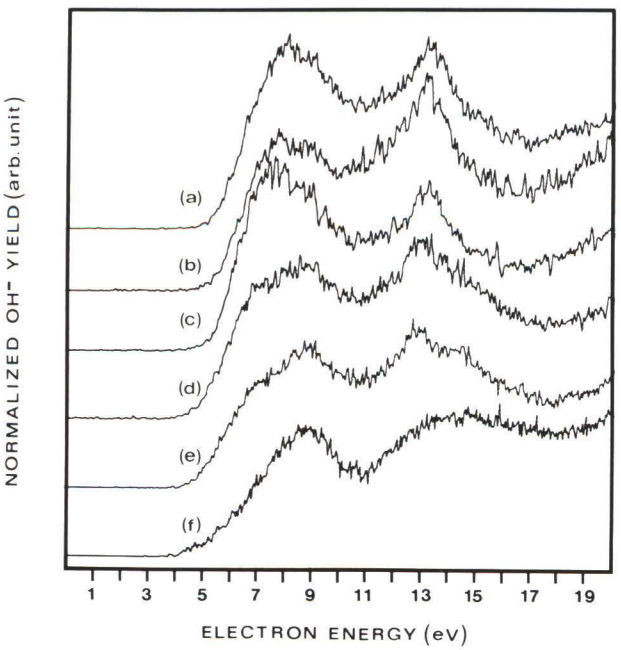

Figure 29. Energy dependence of ESD OH^- yields from 1 layer of (a) C_8H_{18} and (b) C_5H_{12} adsorbed onto 4 ML of O_2; and a film of 5 ML of a mixture of O_2 at 25% volume in (c) C_5H_{12}; (d) C_4H_8; (e) C_3H_6; and (f) C_2H_4.

Here, the O^+ is created with a few eV of KE by the dissociation of a repulsive state. The intermediate N_2O^+ state is also repulsive yielding a NO^+ product with enough KE to overcome the polarization attraction ($\approx$ 0.5 eV) of the positive charge toward the film. The reaction occurs during times characteristic of a vibrational period of the N_2O^+ cation ($\sim 10^{-14}$ sec).

Similar reactions are possible following DEA. In this case, the anion formed with eV's of energy can react rapidly with surrounding molecules and the product anions can be monitored, as a function of electron energy with an ESD apparatus, of the type described in section **III**. The products O_2, NO, and $Ar{\cdot}O^-$ were observed in low-energy ESD from multilayer Ar films deposited on Pt which contained 20% volume N_2O [175]. When the Ar film contained 20% volume of Cl_2, the species Cl_2^- and $Ar{\cdot}Cl^-$ were formed [175]. From ESD experiments on pure multilayer O_2 films, the reaction products O_2^- and O_3^- were detected [180], and in those with O_2 co-adsorbed on Pt with Kr or Ar, the species $Kr{\cdot}O^-$ or $Ar{\cdot}O^-$ were also found to desorb [180]. Surface reactions were also observed in ion-molecule isotope-exchange reactions [11] induced and controlled by low-energy electron impact on mixture films containing 2-6% $^{18}O_2$ in $C^{16}O$. In this energy range, the desorption of $^{16}O^-$ ions demonstrated the occurrence of the $^{18}O^-$ exchange reaction with $C^{16}O$ via a $^{18}O\ C^{16}O^-$

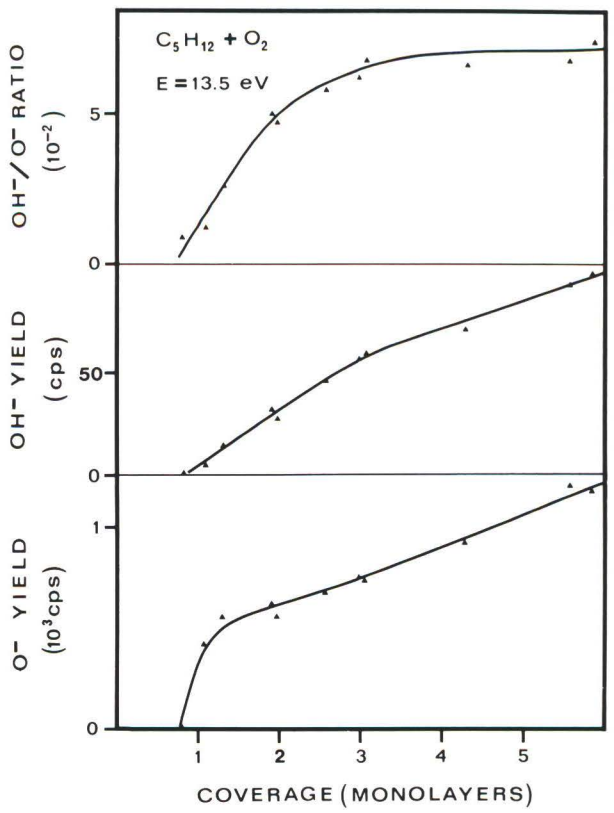

Figure 30. Thickness dependence of the O^- and OH^- yields and OH^-/O^- intensity ratio for a film containing O_2 at 25% volume in n-C_5H_{12} deposited in Pt. The incident electron energy was 13.5 eV.

---

transient anion. The efficiency of the reaction decreased with $^{18}O^-$ KE. Due to multiple electron scattering, this KE was found to be controlled by two parameters, namely, the primary electron energy and the $^{18}O_2$ concentration in the mixture.

When saturated hydrocarbon molecules were condensed onto the surface of multilayer O_2 films grown on Pt, the following abstraction reactions were observed [174, 176]:

$$O^- + C_nH_{2n+2} \rightarrow OH^- + C_nH_{2n+1}\ (n = 1, 2, 4, 5, 6, 7, 8) \quad (R12)$$

in which the O^- ion was provided by DEA in the O_2 layers. From the energetics involved, the O^- ion was found to react with **energies defined by the dissociation limit of the intermediate O_2^- anion.** Similar reactions between condensed O_2 and unsaturated (C_nH_{2n}, n = 2, 3 and 4) hydrocarbon molecules have also been reported [176]. For pentane and 1-butene, the coverage dependence was measured, so that the reaction could be investigated at submonolayer and multilayer coverages. At multilayer coverages, the results were reported for two

different types of co-adsorption: a single layer of hydrocarbons physisorbed on a multilayer O_2 film and a multilayer film composed of a mixture of O_2 and hydrocarbon molecules. In all cases, the substrate was polycrystalline Pt cooled to a temperature of 20K.

The ESD yield of the OH^- product arising from surface reactions induced by low-energy electron impact on various O_2-hydrocarbon mixtures [176] is shown in Figure 29: curves (a) and (b) are for a single ML of n-C_8H_{18} and n-C_5H_{12}, respectively, adsorbed on 4 ML of O_2; while curves (c), (d), (e) and (f) are for a 5 ML of a mixture of O_2 at 25% volume in n-C_5H_{12}, 1-C_4H_8, C_3H_6, and C_2H_4, respectively, condensed on the Pt substrate. Details on the coverage dependence of the O^- and OH^- yields measured from the mixture of O_2 in n-C_5H_{12} are given in Figure 30 for an incident energy of 13.5 eV. The 25%-O_2-1-C_4H_8 mixtures which were investigated over the same thickness range, produced data similar to those shown in Figure 30. The ratio of OH^-/O^- yields defined as the observable efficiency of the reaction leading to OH^- formation, has a maximum value of 0.08 ± 0.01 above 4 ML for 25% volume O_2 in n-C_5H_{12}; at 7.8 eV, the efficiency has the value of 0.016 ± 0.004 for the same coverage. For 1-C_4H_8-O_2, the values are 0.03 ± 0.01 at 13.5 eV and 0.005 ± 0.002 at 7.8 eV.

Since no compound at the film surface contains both hydrogen and oxygen, the OH^- ions in Figure 29 cannot be produced by direct electron impact. However, they can result from surface reactions between ground-state molecules (i.e., O_2 and C_nH_{2n+2} or C_nH_{2n}) and anions produced directly by the electron beam (i.e., O^- and H^- and/or CH_n^-). OH^- can be formed via reaction (R12) in the case of saturated hydrocarbon adsorbates or via the reaction

$$O^- + C_nH_{2n} \rightarrow OH^- + C_nH_{2n-1} \qquad \text{(R13)}$$

when unsaturated hydrocarbons-O_2 mixtures are deposited on Pt. *A priori*, reactions such as

$$H^- + O_2 \rightarrow OH^- + O; \qquad \text{(R14)}$$

and

$$CH_n^- + O_2 \rightarrow OH^- + CH_{n-1}O \qquad \text{(R15)}$$

can also lead to ESD of OH^- since DEA from the deposited hydrocarbons forms H^- and some CH_n^- ions. However, the OH^- yield functions can be correlated to the line shape of the O^- signal and O_2^- dissociation from the states shown in Figure 22. Any OH^- formed by reactions (R14) and (R15) would bear the "signature" of the yield function for H^- and CH_n^- production shown in the examples of Figure 20. In other words, in the case of the most intense ion, desorbing from saturated and unsaturated hydrocarbons (i.e., H^-), the energy dependence of the OH^- yield should resemble the H^- yield function of n-nonane and exhibit a single peak. But this is not the case as seen in Figure 29: the OH^- signal bears the "signature" of DEA from O_2 (i.e., a broad maximum extending from 5 to 10 eV and a peak around 13 eV). From these comparisons, the OH^- signal can be ascribed to reactions (R12) and (R13), since among all ions produced with detectable magnitude, only O^-, can account for the yield functions of Figure 29. Accordingly, the 13 eV structure in Figure 29 curves (a) to (e) arise from reaction of O^- ions formed by a $^2\Sigma^+$ state of O_2. The $^2\Pi_u$ and $^2\Sigma_g^+$ states of O_2, which are resolved in Figure 29 curves (d) and (e), produce O^- ions leading to OH^- products at 7 and 9 eV, respectively. From analysis of the dynamics of this reaction system and comparison with gas-phase behavior, it has been suggested [174] that reactions (R12) and (R13) involve an intermediate step; i.e., the existence of the temporary states $C_nH_{2n+2}O^-$ and $C_nH_{2n}O^-$, that would dissociate into the products of reactions (R12) and (R13), respectively.

From the ratio of the O^- and OH^- yields in Figure 30, the observed efficiency of reaction (R12) is found to increase as a function of thickness (top curve) and saturates above 4 ML. It is of the order of 1% to 7% for a multilayer film (i.e., for an insulating surface). At submonolayer coverage of the reactants (i.e., on a metal surface), this efficiency is reduced by at least an order of magnitude and O^- formation via DEA by more than two orders of magnitude, as shown in Figure 24. The efficiency of reaction (R12) is dependent on the thickness of the hydrocarbon-O_2 mixture film below 4 ML and therefore not directly proportional to the O^- signal. The observable efficiency is affected by different parameters [176] such as the nature of the hydrocarbon molecule, the KE of the reactant O^- ion and the escaping probability of the OH^- ions from the surface. Orientation of the reaction products may also affect the OH^- signal, but this effect is expected to be small compared to the perturbation imposed on dissociation branching and lifetime of the intermediate state $C_5H_{12}O^-$ due to polarization and quenching by the metal, respectively.

X. Summary and Acknowledgments

The information available on low-energy (0-30 eV) electron interactions with atomic and molecular solid films has been reviewed with pertinent examples of the most relevant phenomena. It has been shown that recent advances in slow electron experiments make it possible to obtain reliable information on the scattering, attachment, thermalization and degradation processes involved

in the interaction of secondary electrons within samples irradiated by high energy charged particles. It is hoped that the information assembled in this article can be valuable to the fields of electron microscopy and microanalysis of surfaces, particularly in techniques which utilize low-energy electrons as a primary probe.

The author is indebted to Mrs. Francine Lussier and Mr. Luc Parenteau for their valuable assistance in the preparation of this article. Thanks are also extended to Dr. Michael Huels for suggestions and helpful comments. This work was sponsored by the Medical Research Council of Canada.

References

[1] Allan M (1989) Studies of triplet states and short-lived negative ions by means of electron impact spectroscopy. J. Electr. Spectr. Rel. Phenom. **48**, 219-351.

[2] Apai G, McKenna WP (1991) Surface analysis of polycarbonate thin films by high-resolution electron energy loss spectroscopy: Negative ion resonances and surface vibrations. Langmuir **7**, 2266-2272.

[3] Apai G, McKenna WP (1994) Vibrational structure of polyethylene using high-resolution electron energy loss spectroscopy: Energy dependence and charge neutralization effects. J. Phys. Chem. **98**, 9735-9741.

[4] Arakawa I, Takahoshi M, Takeuchi K (1989) Electron-stimulated desorption of excited neutrals from the surface of solid rare gas. J. Vac. Sci. Technol. A **7**, 2090-2093.

[5] Ashby CIH (1983) Electronic excitation in electron bombardment enhancement of chemical reactions. Appl. Phys. Lett. **43**, 609-611.

[6] Avouris P, Schmeisser D, Demuth JE (1983) Nonradiative relaxation of electronically excited N_2 on Al(111). Comparison with nonlocal optical theory. J. Chem. Phys. **79**, 488-492.

[7] Azria R, Parenteau L, Sanche L (1987) Dynamics of dissociative attachment reactions in electron stimulated desorption: Cl^- from condensed Cl_2. J. Chem. Phys. **87**, 2292-2296.

[8] Azria R, Parenteau L, Sanche L (1987) Dissociative attachment from condensed O_2: Violation of the selection rule $\Sigma^- \nleftrightarrow \Sigma^+$. Phys. Rev. Lett. **59**, 638-640.

[9] Azria R, Parenteau L, Sanche L (1988) Mechanisms for O^- electron stimulated desorption via dissociative attachment in condensed CO. J. Chem. Phys. **88**, 5166-5170.

[10] Azria R, Sanche L, Parenteau L (1989) O^- electron stimulated desorption from O_2 in CO and N_2 matrices. Chem. Phys. Lett. **156**, 606-5170.

[11] Azria R, Parenteau L, Sanche L (1990) Post dissociation interaction in ESD: The $^{18}O^-$-C ^{16}O surface reaction induced by 4-10 eV electrons. Chem. Phys. Lett. **171**, 229-232.

[12] Azria R, Le Coat Y, Ziesel J-P, Guillotin J-P, Mharzi B, Tronc M (1994) Mechanism for resonant O^- electron stimulated desorption from condensed O_2. Non-adiabatic transitions and dynamics. Chem. Phys. Lett. **220**, 417-422.

[13] Bacalis NC, Papaconstantopoulos DA, Pickett WE (1988) Systematic calculations of the band structures of the rare-gas crystals neon, argon, krypton, and xenon. Phys. Rev. B **38**, 6218-6226.

[14] Bader G, Perluzzo G, Caron LG, Sanche L (1982) Elastic and inelastic mean-free-path determination in solid xenon from electron transmission experiments. Phys. Rev. B **26**, 6019-6029.

[15] Bader G, Perluzzo G, Caron LG, Sanche L (1984) Structural-order effects in low-energy electron transmission spectra of condensed Ar, Kr, Xe, N_2, CO and O_2. Phys. Rev. B **30**, 78-84.

[16] Bader G, Chiasson J, Caron LG, Michaud M, Perluzzo G, Sanche L (1988) Absolute scattering probabilities for subexcitation electrons in condensed H_2O. Rad. Res. **114**, 467-479.

[17] Bass AD, Sanche L (1991) Charge trapping by H_2O condensed onto thin films of Kr and Xe. J. Chem. Phys. **95**, 2910-2918.

[18] Bernasconi J, Cartier E, Pfluger P (1988) Hot-electron transport through thin dielectric films: Boltzmann theory and electron spectroscopy. Phys. Rev. B **38**, 12567-12581.

[19] Botelho do Rego AM, Rei Vilar M, Lopes da Silva J, Heyman M, Schott M (1986) Electronic excitation and secondary-electron emission studies by low-energy electrons backscattered from thin polystyrene film surfaces. Surf. Sci. **178**, 367-374.

[20] Botelho do Rego AM, Lopes da Silva JD (1993) End chain segregation effects in polymer surfaces observed by HREELS: A preliminary study. Macromolecules **26**, 4986-4988.

[21] Caron LG, Perluzzo G, Bader G, Sanche L (1986) Electron transmission in the energy gap of thin films of argon, nitrogen, and n-hexane. Phys. Rev. B **33**, 3027-3038.

[22] Cartier E, Pfluger P (1988) Experimental determination of energy dependent inelastic and elastic scattering rates of hot-electrons in large bandgap insulators. Phys. Sci. **T23**, 235-241.

[23] Chang YC, Berry WB (1974) Electron range studies in solid hydrocarbon films at 77K. J. Chem. Phys. **61**, 2727-2735.

[24] Cheng IY, Funabashi K (1973) On the low energy event in Hiraoka-Hamill experiments. J. Chem. Phys. **59**, 2977-2919.

[25] Christophorou LG (1984) Electron-Molecule Interactions and Their Applications. Academic Press, Orlando, FL. pp. 403-423; 477-491.

[26] Cloutier P, Sanche L (1989) A trochoidal spectrometer for the analysis of low-energy inelastically backscattered electrons. Rev. Sci. Instrum. **60**, 1054-1060.

[27] Coletti F, Debever JM, Zimmerer G (1983) Electron-stimulated desorption of solid argon via exciton creation. J. Phys. (Paris) Lett. **45**, L467-L473.

[28] Cui ST, Johnson RE, Cummings PT (1989) Ejection of atoms upon self-trapping of an atomic excitons in solid argon. Phys. Rev. B **49**, 9580-9583.

[29] Daviel S, Wallbank B, Comer J, Hicks PJ (1982) Electron energy-loss spectroscopy of carbon-monoxide using a new position-sensitive multidetector spectrometer: I. The energy region 6-10.9 eV. J. Phys. B **15**, 1929-1937.

[30] Demuth JE, Schmeisser D, Avouris P (1981) Resonance scattering of electrons from N_2, CO, O_2 and H_2 adsorbed on a silver surface. Phys. Rev. Lett. **47**, 1166-1169.

[31] Fain B, Lin SH (1985) Effect of vibrational-energy transfer on laser-induced desorption. Chem. Phys. Lett. **114**, 497-502.

[32] Fano U (1987) Short-range and long-range interactions of slow-electrons in condensed matter: effects on reflection and transmission. Phys. Rev. A **36**, 1929-1931.

[33] Fano U, Stephens JA (1986) Slow electrons in condensed matter. Phys. Rev. B **34**, 438-441.

[34] Fröhlich H (1937) Electric breakdown in ionic crystals. Proc. R. Soc. Ser. A **160**, 230-241.

[35] Fröhlich H, Platzman RL (1953) Energy loss of moving electrons to dipolar relaxation. Phys. Rev. **92**, 1152-1154.

[36] Gardella Jr JA, Pireaux JJ (1990) Analysis of polymer surfaces using electron and ion-beams. Anal. Chem. **62**, A645-A670.

[37] Garten RPH, Werner HW (1994) Trends in applications and strategies in the analysis of thin films, interfaces and surfaces. Anal. Chim. Acta **297**, 3-14.

[38] Goldstein JI, Yakowitz H (1975) Practical Scanning Electron Microscopy. Plenum, New York. pp. 25-28.

[39] Goulet T, Jay-Gerin J-P (1986) Theoretical study of the transmission of low-energy (0-10 eV) electrons through thin-film organic molecular solids: Benzene. Radiat. Phys. Chem. **27**, 229-239.

[40] Goulet T, Pou V, Jay-Gerin J-P (1986) A procedure for determining low-energy ($<$ 10 eV) electron mean free paths in molecular solids: Benzene. J. Electr. Rel. Phenom. **41**, 157-166.

[41] Goulet T, Jay-Gerin J-P, Patau J-P (1987) Monte Carlo simulations of low-energy ($<$ 10 eV) electron transmission and reflection experiments: Application to solid xenon. J. Electr. Rel. Phenom. **43**, 17-35.

[42] Goulet T, Keszei E, Jay-Gerin J-P (1988) Probabilistic description of particle transport. I. General theory of quasielastic scattering in plane-parallel media. Phys. Rev. A **37**, 2176-2182.

[43] Goulet T, Jung J-M, Michaud M, Jay-Gerin J-P, Sanche L (1994) Conduction-band density of states in solid argon revealed by low-energy-electron backscattering from thin films: Role of the electron mean free path. Phys. Rev. B **50**, 5101-5109.

[44] Granville MF, Kohler BF, Snow JB (1981) Franck-Condon analysis of the 1^1A_g-1^1B_u absorption in linear polyenes with two through six double bonds. J. Chem. Phys. **75**, 3765-3769.

[45] Grechov VV (1983) Low-energy ($\leq$ 2 eV) electron escape depths of tetracene films. Chem. Phys. Lett. **96**, 237-242.

[46] Griffith OH, Habliston PA, Birrell GB (1991) Bibliography on emission microscopy, mirror electron microscopy, low-energy electron microscopy and related techniques: 1985-1991. Ultramicroscopy **36**, 262-274.

[47] Hansen W, Bertolo M, Jacobi K (1991) Physisorption of CO on Ag(111) Investigation of the monolayer and the multilayer through HREELS, ARUPS and TDS. Surf. Sci. **253**, 1-12.

[48] Harland PW, Franklin JL (1974) Partitioning of excess energy in dissociative resonance capture processes. J. Chem. Phys. **61**, 1621-1636.

[49] Harrigan ME, Lee HJ (1974) Theory of current characteristics of a thin dielectric film under slow electron impact. J. Chem. Phys. **60**, 4909-4919.

[50] Herzberg G (1966) Spectra of Diatomic Molecules. van Nostrand, New York. pp. 521-522.

[51] Hino S, Sato N, Inokuchi H (1977) Electron escape depths of organic solids. J. Chem. Phys. **67**, 4139-4144.

[52] Hiraoka K (1981) Determination of energies of quasifree electron state V_0 in organic solids from electron transmission spectra., J. Phys. Chem. **85**, 4008-4015.

[53] Hiraoka K, Hamill WH (1972) Characteristic energy losses by slow electrons in organic molecular thin-films at 77K. J. Chem. Phys. **57**, 3870-3881.

[54] Hiraoka K, Hamill WH (1973) Characteristic energy-losses by slow electron impact on thin-film alkanes at 77K. J. Chem. Phys. **59**, 5749-5757.

[55] Hiraoka K, Nara M (1981) Transmission of low-energy electrons through thin-films of benzene and hexane at 80K. Bull. Chem. Soc. Jpn. **54**, 1589-1594.

[56] Hiraoka K, Nara M (1983) Conduction band structure of solid n-alkanes studied by electron-transmission spectra. Chem. Phys. Lett. **94**, 589-591.

[57] Hiraoka K, Nara M (1984) Conduction-band formation through the temporary anion state in organic-solids. Bull. Chem. Soc. Jpn. **57**, 2243-2246.

[58] Hoffman FM, Felter TE, Thiel PA, Weinberg WH (1983) The adsorption of cyclic hydrocarbons on Ru(001) II. cyclohexane. Surf. Sci. **130**, 173-190.

[59] Huang JTJ, Magee JL (1974) On transmission of low-energy electrons in alkane thin films. J. Chem. Phys. **61**, 2736-2739.

[60] Huels MA, Parenteau L, Sanche L (1993) Quenching of the dissociative electron attachment resonances of O_2 physisorbed on amorphous ice. Chem. Phys. Lett. **210**, 340-346.

[61] Huels MA, Parenteau L, Sanche L (1994) Substrate dependence of electron-stimulated O^- yields from dissociative electron attachment to physisorbed O_2. J. Chem. Phys. **100**, 3940-3956.

[62] Huels MA, Parenteau L, Michaud M, Sanche L (1995) Kinetic-energy distributions of O^- produced by dissociative electron attachment to physisorbed O_2. Phys. Rev. A **51**, 337-349.

[63] Hunter SR, Christophorou LG (1984) Electron-attachment to the perfluoroalkanes n-C_nF_{2n+2} (n = 1-6) using high-pressure swarm techniques. J. Chem. Phys. **80**, 6150-6164.

[64] Hussla I, Seki H, Chuang TJ, Gortel ZW, Kreuzer HJ, Piercy P (1985) Infrared-laser-induced photodesorption of NH_3 and ND_3 adsorbed on single-crystal Cu(100) and Ag film. Phys. Rev. B **32**, 3489-3501.

[65] Illenberger E (1981) Measurement of the translational excess energy in dissociative electron attachment processes Chem. Phys. Lett. **80**, 153-158.

[66] Itikawa Y (1974) Electron-impact vibrational excitation of H_2O. J. Phys. Soc. Jpn **36**, 1127-1132.

[67] Jacobi K, Bertolo M (1990) Physisorption of CO and N_2 on Al(111): Observation of surface-molecule vibrations in electron resonance scattering. Phys. Rev. B **42**, 3733-3736.

[68] Jacobi K, Bertolo M, Hansen W (1990) HREELS investigation of physisorbed molecules on single-crystalline surfaces through dipole and resonant electron-scattering mechanism. J. Electr. Spectrosc. Relat. Phenom. **54/55**, 529-540.

[69] Jay-Gerin J-P, Plenkiewicz B, Plenkiewicz P, Perluzzo G, Sanche L (1985) Electron mean free path and conduction-band density-of-state in solid methane as determined from low-energy electron transmission experiments. Sol. State Comm. **55**, 1115-1118.

[70] Kelber JA, Knotek ML (1982) Electron-stimulated desorption of condensed branched alkanes. Surf. Sci. **121**, L499-L506.

[71] Kelber JA, Knotek ML (1984) Electron-stimulated desorption from partially fluorinated hydrocarbon thin films: molecules with common versus separate hydrogen and fluorine bonding sites. Phys. Rev. B **30**, 400-403.

[72] Keszei E, Jay-Gerin J-P, Perluzzo G, Sanche L (1986) Quasielastic hot-electron transport in solid N_2 films. J. Chem. Phys. **85**, 7396-7402.

[73] Keszei E, Goulet T, Jay-Gerin J-P (1988) Probabilistic description of particle transport. II. Analysis of low-energy electron transmission through thin solid Xe and N_2 films. Phys. Rev. A **37**, 2183-2188.

[74] Kimmel GA, Orlando TM, Vézina C, Sanche L (1994) Low-energy electron-stimulated production of molecular hydrogen from amorphous water ice. J. Chem. Phys. **101**, 3282-3286.

[75] Kittel C (1963) Quantum Theory of Solids. Wiley, New York. pp. 137-138.

[76] Kloiber T, Zimmerer G (1989) Recent results from ESD and PSD on rare-gas solids with low-energy and with synchroton radiation excitation. Radiat. Eff. Def. Solids **109**, 219-227.

[77] Knapp M, Echt O, Kreisle D, Recknagel E (1987) Electron-attachment to water clusters under collision-free conditions. J. Phys. Chem. **91**, 2601-2607.

[78] Leclerc G, Goulet T, Cloutier P, Jay-Gerin J-P, Sanche L (1987) Low-energy (0-10 eV) electron transmission spectra of multilayer tryptophan films. J. Phys. Chem. **91**, 4999-5001.

[79] Leclerc G, Cui Z, Sanche L (1987) Effective dissociation cross-section for the low-energy (0.5-31 eV) electron-impact on solid n-hexane thin-films. J. Phys. Chem. **91**, 6461-6463.

[80] Leclerc G, Bass AD, Michaud M, Sanche L (1990) Angle-resolved electron stimulated desorption of metastable atoms from solid Argon. J. Electr. Spectr. Rel. Phenom. **52**, 725-734.

[81] Leclerc G, Bass AD, Mann A, Sanche L (1992) Time-resolved patterns for electron-stimulated desorption of metastable atoms from thin Ar(111) films. Phys. Rev. B **60**, 4865-4873.

[82] Lofthus A, Krupenie PH (1977) Spectrum of molecular nitrogen. J. Phys. Chem. Ref. Data **6**, 113-137.

[83] Magee JL, Helman WP (1977) Energy loss of electrons in random motion. J. Chem. Phys. **66**, 310-318.

[84] Mann A, Leclerc G, Sanche L (1992) Metastable-atom desorption and luminescence stimulated by low-energy electron impact on condensed Kr, Xe and Xe/Kr films. Phys. Rev. B **46**, 9683-9690.

[85] Mann A, Leclerc G, Sanche (1993) Low-energy ESD of metastable atoms from Ar, Kr, Xe(111) condensed films. In: Desorption Induced by Electronic Transition (DIET V). Burns AR, Steckel EB, Jennison DR (eds.). Springer Verlag, Berlin. pp. 329-332.

[86] Mann A, Cloutier P, Liu D. Sanche L (1995)

Excitation-energy transfer and metastable-particle desorption from electron-bombarded Xe films with N_2 and CO top layers. Phys. Rev. B **51**, 7200-7206.

[87] Marsolais RM, Sanche L (1988) Mechanisms producing inelastic structures in low-energy electron transmission spectra. Phys. Rev. B **38**, 11118-11130.

[88] Marsolais RM, Michaud M, Sanche L (1987) Near-threshold electronic excitation by electron impact of multilayer physisorbed N_2 and CO. Phys. Rev. A **35**, 607-618.

[89] Marsolais RM, Deschênes M, Sanche L (1989) Low energy electron transmission method for measuring charge trapping in dielectric films. Rev. Sci. Instr. **60**, 2724-2732.

[90] Marsolais RM, Cartier EA, Pfluger P (1991) Hot electron transport in condensed organic dielectrics. In: Excess Electrons in Dielectric Media. Jay-Gerin J-P, Ferradini C (eds.). CRC Press, Boca Raton, FL. pp. 43-74.

[91] Massey HSW (1976) Negative Ions. University Press, London, U.K. pp. 156-172; 264-272.

[92] McDiarmid R, Sabljic´ A, Doering JP (1985) Valence transition in 1,3-cyclopentadiene, 1,3-cyclohexadiene and 1,3-cycloheptadiene. J. Chem. Phys. **83**, 2147-2152.

[93] McKenna WP, Apai G (1992) Organic polymer surface analysis by high-resolution electron energy loss spectroscopy: Dipole versus nondipole character and resolution enhancement. J. Phys. Chem. **96**, 5902-5907.

[94] Meinke M, Illenberger E (1994) Electron-stimulated desorption of anions from condensed and adsorbed $CFCl_3$ down to very low energies (< 2 eV). J. Phys. Chem. **98**, 6601-6606.

[95] Meinke M, Parenteau L, Rowntree P, Sanche L, Illenberger E (1993) Electron-stimulated desorption of anions from condensed CF_4. Chem. Phys. Lett. **205**, 213-218.

[96] Melton CE (1972) Cross-section and interpretation of dissociative attachment reactions producing OH^-, O^- and H^- in H_2O. J. Chem. Phys. **57**, 4218-4225.

[97] Merkel PB, Hamill WH (1971) Energy loss spectra of low-energy electrons scattered from thin solid molecular films. J. Chem. Phys. **55**, 1409-1413.

[98] Michaud M, Sanche L (1984) Interaction of low-energy electrons (1-30 eV) with condensed molecules: I. Multiple scattering theory. Phys. Rev. B **30**, 6067-6077.

[99] Michaud M, Sanche L (1987) Opening of new decay channels for core-excited resonances. Phys. Rev. Lett. **59**, 645-648.

[100] Michaud M, Sanche L (1987) Total cross sections for slow-electron (1-20 eV) scattering in solid H_2O. Phys. Rev. A **36**, 4672-4683.

[101] Michaud M, Sanche L (1987) Absolute vibrational excitation cross sections for slow-electron (1-18 eV) scattering in solid H_2O. Phys. Rev. A **36**, 4684-4699.

[102] Michaud M, Sanche L (1990) The $^2\Pi_g$ shape resonance of N_2 near a metal surface and in rare gas solids. J. Electr. Spectr. Rel. Phenom. **51**, 237-248.

[103] Michaud M, Sanche L (1994) Low-energy electron-energy-loss spectroscopy of solid films of argon: surface and bulk valence excitons. Phys. Rev. B **50**, 4725-4732.

[104] Michaud M, Sanche L, Gaubert G, Baudoing R (1988) Low-energy electron reflection and transmission on Ar films condensed on polycrystalline platinum. Surf. Sci. **205**, 447-464.

[105] Michaud M, Sanche L, Goulet T, Jay-Gerin JP (1991) Direct observation of the conduction-band density of states in solid argon. Phys. Rev. Lett. **66**, 1930-1933.

[106] Michaud M, Cloutier P, Sanche L (1991) Low-energy electron-energy-loss spectroscopy of amorphous ice: Electronic excitations. Phys. Rev. A **44**, 5624-5627.

[107] Michaud M, Cloutier P, Sanche L (1991) Phonon excitations in low-energy-electron scattering from solid Ar, Kr, and Xe films: Direct observation of conduction-band density of states. Phys. Rev. B **44**, 10485-10492.

[108] Michaud M, Cloutier P, Sanche L (1993) Direct observation of a Feshbach-type electron resonance in solid argon. Phys. Rev. B **47**, 4131-4134.

[109] Michaud M, Cloutier P, Sanche L (1993) Feshbach-type electron resonances in solid Ar, Kr, and Xe films: Decay into multiphonon excitations. Phys. Rev. B **48**, 11336-11346.

[110] Michaud M, Cloutier P, Sanche L (1994) Phonon excitations in low-energy electron resonant scattering from solid films of N_2. Phys. Rev. B **49**, 8360-8366.

[111] Michaud M, Fraser M-J, Sanche L (1994) Low-energy electron-energy-loss spectroscopy of solid methanol: Vibrational and electronic excitations. J. Chim. Phys. **91**, 1223-1227.

[112] Mills DL (1992) Resonant scattering of slow-electron in molecular solids: Suppression of the elastic beam. Phys. Rev. B **45**, 36-42.

[113] Momose M, Kamiya K, Sugita K, Ueno N (1994) Growth and stability of H_2-phthalocyanine thin films on MoS_2 surfaces studied by means of low-energy electron transmission spectroscopy. Jpn. J. Appl. Phys. **33**, 4754-4758.

[114] Mott NF, Massey HSW (1989) The Theory of Atomic Collisions. Clarendon Press, Oxford. pp. 362-608.

[115] Noell JO, Melius CF, Stulen RH (1985)

Mechanisms of electron-stimulated desorption of protons from water: Gas, chemisorbed and ice phases. Surf. Sci. **157**, 119-150.

[116] Oeter D, Egelhaaf H-J, Ziegler Ch, Oelkrug D, Göpel W (1994) Electronic transitions in α-oligothiophene thin films. Comparison of ultraviolet/visible absorption spectroscopy and high resolution electron energy loss spectroscopy investigations. J. Chem. Phys. **101**, 6344-6352.

[117] Oster T, Kuhn A, Illenberger E (1989) Gas-phase negative-ion chemistry. Int. J. Mass. Spectrom. Ion Processes **89**, 1-72.

[118] Oster T, Ingolfsson O, Meinke M, Jaffke T, Illenberger E (1993) Anion formation from gaseous and condensed CF_3I on low energy electron impact. J. Chem. Phys. **99**, 5141-5150.

[119] Palmer RE (1992) Electron-molecule dynamics at surfaces. Prog. Surf. Sci. **41**, 51-108.

[120] Palmer RE, Rous PJ (1992) Resonances in electron-scattering by molecules on surfaces. Rev. Mod. Phys. **64**, 383-440.

[121] Parenteau L, Sanche L (1994) L'attachement dissociatif d'électrons de faible énergie (0-20 eV) sur le méthanol et diverses molécules organiques {Dissociative attachment of low energy (0-20 eV) electrons to methanol and various organic molecules}. J. Chim. Phys. **91**, 1237-1242 (in French).

[122] Parenteau L, Jay-Gerin J-P, Sanche L (1994) Electron-stimulated desorption of H^- ions via dissociative electron attachment in condensed methanol. J. Phys. Chem. **98**, 10277-10281.

[123] Perluzzo G, Bader G, Caron LG, Sanche L (1982) Temperature dependence of some structures in electron transmission spectra of Xe solid films. Phys. Rev. B **26**, 3976-3928.

[124] Perluzzo G, Sanche L, Gaubert C, Baudoing R (1984) Thickness-dependent interference structure in the 0-15 eV electron transmission spectra of rare-gas films. Phys. Rev. B **30**, 4292-4296.

[125] Perluzzo G, Bader G, Caron LG, Sanche L (1985) Direct determination of electron band energies by transmission interference in thin films. Phys. Rev. Lett. **55**, 545-548.

[126] Peterson OG, Batchelder DN, Simmons RO (1966) Measurements of x-ray lattice constant, thermal expansivity and isothermal compressibility of argon crystals. Phys. Rev. **150**, 703-711.

[127] Pfluger P, Zeller HR, Bernasconi J (1984) Hot-electron transport in polymeric dielectrics. Phys. Rev. Lett. **53**, 94-97.

[128] Pimblott SM, Laverne JA, Mozumder A, Green NJB (1990) Structure of electron tracks in water. 1. Distribution of energy deposition events. J. Phys. Chem. **94**, 488-495.

[129] Pireaux JJ, Thiry P, Caudano R, Pfluger P (1986) Surface analysis of polyethylene and hexatriacontane by high resolution electron energy loss spectroscopy. J. Chem. Phys. **84**, 6452-6457.

[130] Pireaux JJ, Thiry PA, Sporken R, Caudano R (1990) Analysis of semiconductors and insulators by high-resolution electron-energy loss spectroscopy: Prospects for quantification. Surf. Interf. Anal. **15**, 189-205.

[131] Pireaux JJ, Vermeersh M, Caudano R (1992) Studies of insulators with HREEL spectroscopy. J. Electr. Spectr. Rel. Phenom. **59**, 33-48.

[132] Plenkiewicz B, Plenkiewicz P, Perluzzo G, Jay-Gerin J-P (1985) Analysis of low-energy electron transmission experiments through thin solid xenon films in the elastic scattering region. Phys. Rev. B **32**, 1253-1256.

[133] Plenkiewicz P, Jay-Gerin J-P, Plenkiewicz B, Perluzzo G (1986) Electron mean free path and conduction-band density of states in solid argon. Sol. State Comm. **57**, 203-205.

[134] Plenkiewicz B, Plenkiewicz P, Jay-Gerin J-P (1986) Energy dependence of the mean free path of excess hot electrons in solid xenon in the elastic scattering region. Phys. Rev. B **33**, 5744-5746.

[135] Plenkiewicz P, Plenkiewicz B, Jay-Gerin J-P (1988) Conduction-band density of states of solid argon. Sol. State Comm. **65**, 1227-1230.

[136] Powell CJ (1984) Inelastic scattering of electrons in solids. In: Electron Beam Interaction with Solids. Kyser DF, Niedrig H, Newbury DE, Shimizu R (eds.). Scanning Electron Microscopy, Inc., A.M.F. O'Hare (Chicago), IL. 19-31.

[137] Ray AK, Trickey SB (1981) Augmented-plane-wave to Gaussian-orbital conversion procedure: One-electron states and Compton profiles of fcc neon. Phys. Rev. B **24**, 1751-1760.

[138] Ray AK, Trickey SB (1983) Augmented-plane-wave to Gaussian-orbital conversion procedure: One-electron states and Compton profiles of fcc neon. Phys. Rev. B **28**, 7352-7352.

[139] Rei Vilar M, Heyman M, Schott M (1983) Spectroscopy of low-energy electrons backscattered from an organic-solid surface: Pentacene. Chem. Phys. Lett. **94**, 522-526.

[140] Rei Vilar M, Schott M, Pireaux JJ, Grégoire C, Thiry PA, Caudano R, Lapp A, Botelho do Rego AM, Lopes da Silva JD (1987) Study of polymer film surfaces by EELS using selectively deuterated polystyrene. J. Surf. Sci. **189/190**, 927-934.

[141] Rei Vilar M, Blatter G, Pfluger P, Heymann M, Schott M (1988) Monoenergetic and directed electron emission from a large-bandgap organic insulator with negative electron affinity. Europhys. Lett. **5**, 375-380.

[142] Rei Vilar M, Schott M, Pireaux JJ, Grégoire C, Caudano R, Thiry PA, Lapp A, Lopes da Silva JD, Botelho do Rego AM (1989) Film of mixtures of deuterated and hydrogenated polymers - an HREELS study. Surf. Sci. **211/212**, 782-789.

[143] Rei Vilar M, Schott M, Pfluger P (1990) Vibrational and electronic excitation of hexatriacontane thin-films by low-energy electron impact. J. Chem. Phys. **92**, 5722-5730.

[144] Rei Vilar M, Botelho do Rego AM, Lopes da Silva JD, Abel F, Quillet V, Schott M, Petitjean S, Jérôme R (1994) Quantitative analysis of polymer surfaces and films using elastic recoil detection analysis (ERDA), Fourier transform infrared spectroscopy (FTIRS), and high-resolution electron energy loss spectroscopy (HREELS). Macromolecules **27**, 5900-5906.

[145] Reimann CT, Johnson RE, Brown WL (1984) Sputtering and luminescence in electronically excited solid argon. Phys. Rev. Lett. **53**, 600-603.

[146] Reimann CT, Brown WL, Grosjean DE, Nowakowski MJ (1992) Dimer desorption from solid argon films electronically excited by MeV He ions. Phys. Rev. B **45**, 43-55.

[147] Rosenberg RA, Rehn V, Knotek ML, Stulen RH (1987) Photon-stimulated desorption and electron-stimulated desorption of H^+ from solid H_2O and NH_3. J. Vac. Sci. Technol. A **5**, 1085-1086.

[148] Rowntree P, Parenteau L, Sanche L (1991) Energy and charge transfer at rare-gas surfaces via substrate excitation and core-excited resonances. Chem. Phys. Lett. **182**, 479-485.

[149] Rowntree P, Parenteau L, Sanche L (1991) Electron stimulated desorption via dissociative attachment in amorphous H_2O. J. Chem. Phys. **94**, 8570-8576.

[150] Rowntree P, Parenteau L, Sanche L (1991) Dielectric polarization invariance in dissociative electron attachment from condensed saturated hydrocarbons. J. Phys. Chem. **95**, 523-524.

[151] Rowntree P, Parenteau L, Sanche L (1991) Anion yield produced by low-energy electron impact on condensed hydrocarbon films. J. Phys. Chem. **95**, 4902-4909.

[152] Rowntree P, Sambe H, Parenteau L, Sanche L (1993) Formation of anionic excitations in the rare-gas solids and their coupling to dissociative states of adsorbed molecules. Phys. Rev. B **47**, 4537-4554.

[153] Rowntree P, Sanche L, Parenteau L, Meinke M, Weik F, Illenberger E (1994) Dissociative electron attachment to condensed and adsorbed halomethanes. J. Chem. Phys. **101**, 4248-4259.

[154] Sakurai M, Okano T, Tuzi Y (1987) Vibrational excitation of physisorbed CO_2 on a Ag(111) surface. J. Vac. Sci. Technol. A **5**, 431-434.

[155] Sambe H, Ramaker DE (1987) The σ^- selection rule in electron attachment and autoionization of diatomic molecules. Chem. Phys. Lett. **139**, 386-389.

[156] Sambe H, Ramaker DE (1992) Dissociative electron attachment of O_2: a solid-state effect on potential curve crossing. Surface Sci. **269**, 444-451.

[157] Sambe H, Ramaker DE, Parenteau L, Sanche L (1987) Image-charge effects in electron-stimulated desorption: O^- from O_2 condensed on Ar films grown on Pt. Phys. Rev. Lett. **59**, 236-239.

[158] Sambe H, Ramaker DE, Parenteau L, Sanche L (1987) Electron-stimulated desorption enhanced by coherent scattering. Phys. Rev. Lett. **59**, 505-508.

[159] Sambe H, Ramaker DE, Deschênes M, Bass AD, Sanche L (1990) Absolute cross section for dissociative electron attachment in O_2 condensed on Kr film. Phys. Rev. Lett. **64**, 523-526.

[160] Sanche L (1979) Transmission of 0-15 eV monoenergetic electrons through thin-film molecular solids. J. Chem. Phys. **71**, 4860-4882.

[161] Sanche L (1981) Low-energy electron stimulated desorption from condensed molecules. Comm. Atom. Mol. Phys. **26**, 321-332.

[162] Sanche L (1984) Dissociative attachment in electron scattering from condensed O_2 and CO. Phys. Rev. Lett. **53**, 1638-1641.

[163] Sanche L (1988) Dissociative attachment in ESD from condensed molecules. In: Desorption Induced by Electronic Transitions (DIET III). Springer Ser. in Surface Sci. **13**. Stulen RH, Knotek ML (eds.). Springer-Verlag, Berlin, Germany. pp. 78-84.

[164] Sanche L (1992) Dissociative attachment and surface reactions induced by low-energy electrons. J. Vac. Sci. Technol. B **10**, 196-200.

[165] Sanche L, Deschênes M (1988) Mechanisms of charge trapping at a dielectric surface: Resonance stabilization and dissociative attachment. Phys. Rev. Lett. **61**, 2096-2098.

[166] Sanche L, Michaud M (1981) Electron energy-loss vibronic spectroscopy of matrix-isolated benzene and multilayer benzene films. Chem. Phys. Lett. **80**, 184-187.

[167] Sanche L, Michaud M (1981) Vibrational excitation via shape resonances in electron scattering from N_2 multilayer films. Chem. Phys. Lett. **84**, 497-500.

[168] Sanche L, Michaud M (1981) Resonance-enhanced vibrational excitation in electron scattering from O_2 multilayer films. Phys. Rev. Lett. **47**, 1008-1011.

[169] Sanche L, Michaud M (1983) Vibrational structure in the N_2^- ($^2\Pi_g$) electron resonance of N_2 films. Phys. Rev. B **27**, 3856-3858.

[170] Sanche L, Michaud M (1984) Interaction of low-energy electrons (1-30 eV) with condensed mole-

cules: II. Vibrational-librational excitation and shape resonances in thin N_2 and CO films. Phys. Rev. B **30**, 6078-6092.

[171] Sanche L, Michaud M (1984) Vibrational-librational excitation and shape resonances in electron scattering from condensed N_2, CO, and NO. In: Resonances in Electron-Molecules Scattering van der Waals Complexes and Reactive Chemical Dynamics. Truhlar DG (ed.). ACS Symp. Series no **263**, 211-228.

[172] Sanche L, Michaud M (1984) Vibrational excitation via shape resonances in electron scattering from the NO dimer. J. Chem. Phys. **81**, 257-261.

[173] Sanche L, Parenteau L (1986) Dissociative attachment in electron-stimulated desorption from condensed NO and N_2O. J. Vac. Sci. Technol. A **4**, 1240-1242.

[174] Sanche L, Parenteau L (1987) Ion-molecule surface reactions induced by slow (5-20 eV) electrons. Phys. Rev. Lett. **59**, 136-139.

[175] Sanche L, Parenteau L (1989) Production of anion-atom complexes by electron stimulated desorption. J. Chem. Phys. **90**, 3402-3403.

[176] Sanche L, Parenteau L (1990) Surface reactions between O_2 and hydrocarbons induced by dissociative electron attachment. J. Chem. Phys. **93**, 7476-7482.

[177] Sanche L, Bader G, Caron L (1982) Transmission of 0-15 eV monoenergetic electrons through aliphatic and alicyclic hydrocarbon films, J. Chem. Phys. **76**, 4016-4027.

[178] Sanche L, Perluzzo G, Bader G, Caron LG (1982) Temperature and thickness dependence of the 0-15 eV electron transmission spectra of rare gas films. J. Chem. Phys. **77**, 3285-3286.

[179] Sanche L, Perluzzo G, Michaud M (1985) Electron transmission spectroscopy of matrix-isolated N_2. J. Chem. Phys. **83**, 3837-3842.

[180] Sanche L, Parenteau L, Cloutier P (1989) Dissociative attachment reactions in electron stimulated desorption from condensed O_2 and O_2-doped rare-gas matrices. J. Chem. Phys. **91**, 2664-2674.

[181] Sanche L, Bass AD, Parenteau L, Gortel ZW (1993) Measuring diffusion in thin films by dissociative electron attachment: O_2 in Kr. Phys. Rev. B **48**, 5540-5548.

[182] Schmeisser D, Demuth JE, Avouris P (1982) Electron-energy-loss studies of physisorbed O_2 and N_2 on Ag and Cu surfaces. Phys. Rev. B **26**, 4857-4863.

[183] Schulz GJ (1973) Resonances in electron impact on atoms. Rev. Mod. Phys. **45**, 378-422.

[184] Schulz GJ (1973) Resonances in electron impact on diatomic molecules. Rev. Mod. Phys. **45**, 423-486.

[185] Silva LA, Palmer RE (1992) Resonant electron-stimulated desorption of O^- ions from oriented O_2 on graphite. Surface Sci. **282**, 313-317.

[186] Squillacote ME, Sheridan RS, Chapman OL, Anet FAL (1979) Planar S-cis-1.3 butadienne J. Am. Chem. Soc. **101**, 3657-3659.

[187] Steinberger IT, Bass AD, Shechter R, Sanche L (1993) Low-energy electron transmission in solid krypton and xenon films. Phys. Rev.B **48**, 8290-8298.

[188] Stockbauer R, Bertel E, Madey TE (1982) The origin of H^+ in electron stimulated desorption of condensed CH_3OH. J. Chem. Phys. **76**, 5639-5641.

[189] Stulen RH, Thiel PA (1985) Electron-stimulated desorption and thermal desorption spectrometry of H_2O on Ni (111). Surf. Sci. **157**, 99-118.

[190] Swiderek P, Michaud M, Hohlneicher G, Sanche L (1990) Electron-energy-loss spectroscopy of solid naphthalene and acenaphtene: Search for the lowest triplet states. Chem. Phys. Lett. **175**, 667-673.

[191] Swiderek P, Michaud M, Hohlneicher G, Sanche L (1991) Electron-energy-loss spectroscopy of solid phenanthrene and biphenylene: Search for the low-lying triplet states. Chem. Phys. Lett. **178**, 289-294.

[192] Swiderek P, Michaud M, Hohlneicher G, Sanche L (1991) Electron energy-loss spectroscopy of solid fluorene and biphenyl: Search for the low-lying triplet states. Chem. Phys. Lett. **187**, 583-589.

[193] Swiderek P, Michaud M, Sanche L (1993) Electron-energy-loss spectroscopy of condensed butadiene and cyclopentadiene: Vibrationally resolved excitation of the low-lying triplet states. J. Chem. Phys. **98**, 8397-8405.

[194] Swiderek P, Fraser M-J, Michaud M, Sanche L (1994) Electron-energy-loss spectroscopy of low-lying triplet states of styrene. J. Chem. Phys. **100**, 70-77.

[195] Taguchi Y, Daté M, Takagi N, Aruga T, Nishijima M (1994) Adsorbed states of NH_3 and C_6H_6 on the Si(111)($\sqrt{3} \times \sqrt{3}$)R30°-B surface: Thermal-desorption and electron-energy-loss spectroscopy studies. Phys. Rev. B **50**, 17440-17449.

[196] Takayanagi K (1967) Scattering of slow electrons by molecules. Prog. Theor. Phys. Jpn. Suppl. **40**, 216-248.

[197] Thiel PA, Hoffmann FM, Weinberg WH (1981) Monolayer and multilayer adsorption of water on Ru(001). J. Chem. Phys. **75**, 5556-5572.

[198] Tolk NH, Traum MM, Tully JC, Madey TE (1983) Desorption Induced by Electronic Transitions. Springer Ser. in Chem. Phys. **24**. Springer-Verlag, New York. pp. 262-266.

[199] Ueno N, Sugita K, Seki K, Inokuchi H (1986) Low-energy electron transmission and secondary-electron emission experiments on crystalline and molten long-chain alkanes. Phys. Rev. B **34**, 6386-6393.

[200] Ueno N, Suzuki K, Momose M, Kushida M, Sugita K (1994) Growth of Pb-phthalocyanine thin films

on MoS_2 surfaces studies by means low-energy electron transmission spectroscopy. Jpn. J. Appl. Phys. **33**, 319-323.

[201] Wandass JH, Gardella Jr JA (1985) High resolution electron energy loss spectroscopy of fatty acids prepared by Langmuir-Blodgett techniques on polycrystalline silver. Surf. Sci. **150**, L107-L114.

[202] Wandass JH, Gardella Jr JA (1987) Vibrational spectroscopic analysis of Langmuir-Blodgett multilayers by HREELS - Sampling depth and scattering mechanisms. Langmuir **3**, 183-188.

[203] Wethi E, Erbudak M, Vvedensky DD (1994) Secondary-electron imaging of disordered submonolayers. Surf. Sci. **317**, 235-240.

[204] Winters HF (1975) Dissociation of methane by electron impact. J. Chem. Phys. **63**, 3462-3466.

[205] Winters HF (1979) Dissociation of ethane by electron impact. Chem. Phys. **36**, 353-364.

[206] Zimmerer G (1987) Creation, motion and decay of excitons in rare-gas solids. In: Excited-State Spectroscopy in solids. Grassano U, Terzi N (eds.). North-Holland, Amsterdam, Netherlands. pp. 37-110.

Discussion with Reviewers

K. Goto: We tacitly assume that the secondary electrons are distributed in the energy range up to 50 eV and have a maximum appearing several eV's below, though you say 70 eV and 10 eV, respectively. I have observed, for some pure metals and semiconductors, SE characteristics in an absolute manner using an electrometer, but the maximum was always observed at the 10 eV or below in "E N(E)" mode. Thus, the real maximum should exist around a few eV.

Author: In this paper, when I refer to secondary electrons I mean "true" secondary electrons; that is to say, those which are produced as the direct result of the interaction of fast charged particles within the target. Their distribution cannot be completely measured experimentally but can usually be estimated from optical oscillator strengths. It exhibits a maximum in the 8-10 eV range for water and organic material. What is often called the secondary electron distribution is the one obtained by measuring the energies of the flux of electrons emanating from a bombarded surface. Such a distribution contains, in addition to the "true" secondary electrons, those produced by ionization by the true secondaries, the tertiary electrons, and so on... Such a distribution is expected to peak at energies lower than 8-10 eV, sometimes as low as 2 eV.

K. Goto: Experiments in the range 1-30 eV are quite difficult. Many effects such as those due to space charge, local charging of the sample and instrument, regional work function changes, residual magnetic field (even 1 mG), contamination on the instruments, etc., could easily change and alter the results. Organic materials are always a cause of contamination. My main concern is the reproducibility of results. Do you use reference material(s) prior to the experiments on new materials? Please tell us more about your superb technique.

Author: I am pleased to realize that you appreciate the difficulties involved in doing low-energy electron experiments on condensed organic material. We always use the purest possible material which is first transferred to a small high vacuum system where it is degassed by freeze-thaw-heat cycles; after small amounts are vaporized into the main ultra-high-vacuum system in front of the cooled substrate. If during the experiment, charging causes a deviation by more than 50 meV in the energy scale, a new film is deposited. Reproducibility is always verified many times on the sample at various thicknesses and by scanning the energy in both directions. Rare gases, N_2 and C_6H_6 have now become our reference compounds.

J.D. Brown: The review deals only with thin films deposited on metallic substrates. Except for the electron transmission experiments, most of the other techniques can be applied to bulk specimens. Are there reasons why measurements on bulk materials are excluded?

Author: Yes, it is because the total mean free paths of low-energy electrons is fairly small. For most measurements, the data do not change appreciably beyond thicknesses (l) larger than about 20 monolayers, indicating that most interactions occur in the surface region and that $l = \infty$ would not yield much different results.

J.D. Brown: Concerning charge trapping, I would have thought that currents of 10^{-9} A would have caused immediate charging problems. The data seem to show that undistorted spectra are obtained in the rather long time of 0.1 seconds. Are there special experimental precautions that had to be taken?

Author: Yes, insulators and dielectrics are usually found to charge more rapidly than shown in our results. However, in principle, for a perfect insulator injected with electrons in its **conduction band** no charging should occur at all. In practice, electrons lose energy and are trapped at geometrical defects or chemical impurities. Therefore, it is a question of purity and ordering; for highly pure Kr (99.9995%) condensed into the (111) orientation, very little trapping exists below about 100 layers.

J.D. Brown: In the electron transmission spectra of n-hexane (Fig. 7), additional structure appears at the higher temperatures above 60K. I assume that these are repeated spectra from the same film gradually warmed. Was the film cooled back from the higher temperature and a repeat spectrum obtained at 15K? I would expect

that the spectrum would then show the additional structures at the low temperature and that this would confirm the interpretation of the development of a crystalline component.

Author: No, these were different films cooled and held during the experiment at the temperatures specified in Figure 7. The experiment you suggest has been performed with rare gases [123, 178] and confirms your prediction.

G.F. Rempfer: In the first paragraph of section **II**, should **amplitude** by replaced by **intensity**?

Author: No, amplitude cannot, in this case, be replaced by intensity which would be proportional to the square of the electron wave amplitude.

G.F. Rempfer: Does significant specimen damage occur for electron energies below 3 eV?

Author: In all the compounds we have studied so far, we did not find specimen damage for electron energies below 3 eV, except for halogenated compounds for which DEA is possible below 3 eV. In certain compounds such as CCl_4, even a 0 eV electron can cause dissociation ($e + CCl_4 \rightarrow CCl_4^- \rightarrow Cl^- + CCl_3$).

D. Roy: You say that conduction in gap states explains the sharp peak near 0 eV of Figure 7 for n-hexane. Could you be more explicit?

Author: LEET spectra usually exhibit a sharp rise near 0 eV which reflects the beginning of transmission (i.e., the fact that electrons near 0 eV can start penetrating the film). In Figure 7, this rise can be seen around 1 eV but it is preceded by a sharp peak. Analysis of the intensity of that latter peak and the rest of the LEET spectrum as a function of film thickness indicates two different behaviors [21]. The rest of the spectrum shows quasi-elastic scattering behavior whereas transmission in the peak can be described by trap to trap conduction [21]. From this analysis, the lowest conduction level has been fixed at 0.8 eV for solid n-hexane.

D. Roy: Induction of chemical reactions by low energy electrons can lead to special technological applications. Could you give some examples?

Author: The most obvious application is the induction of a specific chemical reaction by the tip of a scanning tunnelling microscope via DEA. This would allow to "write" a chemical reaction on a nanometer scale. The technique is briefly described in a recent paper (Di *et al.*, Energy-selective reaction of the hydrogen-passivated Si surface with carbon tetrafluoride via dissociative electron attachment, Phys. Rev. B, in press) where we show that DEA to CF_4 physisorbed on a hydrogenated Si surface leads to fluorination of that surface via specific reactions.

D. Roy: You have presented many results on dissociative attachment and you state that this is an important process for damage to molecular and organic solids. Is there any reason to believe that dissociative attachment would be more efficient than dissociation via electronic excitation and dissociation via ionization to induce such damage?

Author: Below the threshold for dipolar dissociation, molecular dissociation can occur via a neutral excited state or a transient anion (TI). However, since electron scattering in the low energy range is usually dominated by the formation of TI, so is also the dissociation of molecules. In other words, the probability to form a transient anion at low energies is usually larger than that to produce an electronic excited state by direct scattering; this is seen in the vibrational excitation cross-section of condensed molecules (i.e., Figs. 9 and 10). Above the dipolar dissociation threshold, dissociation via electronic and ionized states starts to dominate at certain energies which may be beyond those considered in the present review article.

M. Allan: Concerning the principle of the LEET spectroscopy: the total current collected must be equal to the current leaving the beam source, and thus constant. Am I correct in assuming that the principle of operation involves splitting the incident beam at or near the surface into a portion which penetrates deep into the film and is eventually collected on the metal plate below it, and a portion which, after being (mostly inelastically) scattered by atoms and molecules near the surface, returns into the vacuum and is collected by surrounding metal parts? LEET thus measures this "splitting ratio". What is the typical fraction of current which is transmitted? Is the following simple interpretation of the LEET spectrum correct? The electrons with energies where the CDOS is high (or where the virtual orbitals are, if the film were a single large molecule) scatter less and are conducted through the film, whereas electrons outside the high CDOS scatter more and are more likely to return to the vacuum?

Author: Yes, you are correct in assuming that the principle of operation of LEET spectroscopy involves splitting the total beam current into a portion which reaches the metal substrate and a portion which returns to vacuum. A LEET spectrometer has an added set of deflector plates at the exit of the trochoidal monochromator which allows to "dump" the reflected beam outside the target axis, to make sure that we are not recording any multiply reflected current.

The amount of transmitted current is strongly dependent on electron energy. In the 0-2 eV region, it can be as high as 80% of the total current because electrons scattered near the surface have their velocity vector reoriented with respect to their primary axis. At low energies, the component of the reoriented vector parallel to

the surface normal (i.e., to the incident beam direction) is often too small to overcome the induced polarization potential. In other words, electron refraction increases the transmitted current.

The penetration of electrons in the film is proportional to the CDOS (e.g., if no state is available in the film for the electron, it cannot penetrate the film). I guess, from a gas-phase analogy, that this could be seen as elastic scattering as you explain.

M. Allan: Resonances are now recognized to be essential for a high yield of electronically excited states (at least for spin-forbidden transitions) both in the gas phase and for molecules on surfaces. Are they also important for electronic excitation in the bulk? An important mechanism for the very elegant metastable desorption experiment discussed by the author in connection with Figures 14-16 is electronic excitation in the bulk, followed by exciton migration toward the surface, where they cause desorption. Is the excitation in the bulk resonant? In other words, are the peaks 2-3 eV above threshold in Figures 17 and 18 resonances?

Author: From our data on threshold electronic excitation of N_2 and CO [87, 88] which resemble the gas-phase results, I would say, yes; resonances are also important to create bulk and surface excitons. The peaks in Figures 17 and 18 could derive from broad resonances but this would be difficult to prove.

M. Allan: Excitation of vibrational overtones of the $a^1\Delta_g$ states is observed at 9 eV in Figure 9, in contrast to observations in the gas phase. Could this also be a manifestation of the activity of resonances such as Σ_g^+, which are inactive in the gas phase because attachment is symmetry forbidden?

Author: Yes, it could very well arise from decay of the Σ^+ states whose presence we only discovered after our work on vibrational excitation in O_2. We are now redoing the condensed O_2 experiment with this in mind and your recent O_2 data.

M. Allan: The excitation functions for vibrational excitation on rare gas films or matrices, such as shown for N_2 in Figures 10 and 11 are very revealing. Why is such an excitation function not shown for O_2 in the $^2\Pi_g$ resonance region?

Author: Because no resonance is observed in the 0.5-2 eV region with electron spectrometers. This is probably due to the polarization energy which is expected to shift the $^2\Pi_g$ state at about 1.5 eV below the vacuum level. We cannot work below 0.5 eV with our spectrometers but the charging experiment suggest the presence of a resonance below 0.5 eV [165].

M. Allan: What is the connection between the repulsive force between Ar and Ar^* on the one hand and the negative electron affinity of bulk Ar on the other?

Author: Creating an Ar^* is like trying to squeeze an electron in the band gap of the solid. The lower the electron affinity, the larger is the band gap and the greater is the repulsive force on the excited electron and hence between Ar^* and the surrounding atoms.

M. Allan: Would it be possible, or will it become possible in the future, to give absolute values for the vibrational and electronic excitation and desorption processes (such as shown in Figures 10, 11 and 15)?

Author: We have already measured absolute cross-sections for vibrational excitation of all intramolecular and phonon modes in amorphous H_2O in the incident energy range 1.5-18 eV [101] and absolute dissociative attachment (DA) cross-sections in O_2 [159] and CF_4 (Fig. 27). Other absolute DA measurements in CH_3Cl and CO_2 will soon appear (Huels MA, Bass AD, Ayotte P, Sanche L, Absolute cross sections for anion production by low energy electron impact on physisorbed CO_2, Chem. Phys. Lett., in press; Sanche L, Bass AD, Ayotte P, Fabrikant II, The effect of the condensed phase on dissociative electron attachment: CH_3Cl, Phys. Rev. Lett., in press).

M. Allan: The lack of O^- yield for O_2 on H_2O in Figure 25 is striking. The most striking difference between H_2O and the other supports, from a chemical point of view, is that H_2O is a protic solvent, i.e. it is slightly acidic. Could it be that the O_2^- resonances are rapidly quenched by acid-base reaction to form O_2H^-? (The test would be trying other protic solvents such as methyl-alcohol, or formic acid).

Author: This is similar to what I think. Either the electron is rapidly attracted to the positive end of the permanent dipole of H_2O and leaves O_2 before dissociation; or, the proton jumps rapidly on the O_2^- forming O_2H. We will try your suggestion.

M. Allan: In connection with the n-hexane loss experiment shown in Figure 28, I find it interesting to observe that the shape of the signal below 7 eV is reminiscent of the shape of the resonant vibrational excitation in n-propane (I think that n-propane and n-hexane are about equivalent for this purpose) {M. Allan, CHIMIA **48** (1994) 372-377}. This would support the conclusion of the author, that the loss is caused by evaporation induced by (resonant) vibrational excitation.

Author: I agree. Thank you for pointing out this comparison.

M. Allan: Resonant enhancement of vibrational and electronic excitation in O_2 at 20 eV is reported in Figure 9. What resonance is this?

Author: The residual vibrational excitation at 20 eV is due to the tail of the "9 eV" resonance. In the condensed phase, this resonance is very broad as seen from the excitation function [168].